Amine functionalized electrically conductive core-sheath MEH-PPV:PCL electrospun nanofibres for enhanced cell-biomaterial interactions

Rajiv Borah[1], Ganesh C. Ingavle[2,3], Susan R. Sandeman[2], Ashok Kumar[1,], Sergey V. Mikhalovsky[4,5]*

AUTHOR ADDRESS: [1]Materials Research Laboratory, Department of Physics, Tezpur University, Tezpur, 784028, India

[2]Biomaterials and Medical Devices Research Group, School of Pharmacy and Biomolecular Sciences, Huxley Building, University of Brighton, Brighton BN2 4GJ, UK

[3]Symbiosis Centre for Stem Cell Research, Symbiosis School of Biological Sciences, Symbiosis International University, Pune, 412115, India

[4]ANAMAD Ltd, Sussex Innovation Centre,Science Park Square, Falmer,Brighton BN1 9SB, UK

[5]SD Asfendiyarov Kazakh National Medical University, Tole Bi Street 94, Almaty, 050000, Kazakhstan

*Ashok Kumar, Ph.D. (Corresponding author)

Materials Research Laboratory, Department of Physics, Tezpur University, Tezpur-784028, India

Phone: +91-3712-275553

E-mail: ask@tezu.ernet.in

KEYWORDS: Conducting polymer, MEH-PPV, Surface functionalization, Electrical stimulation, Neural tissue engineering.

ABSTRACT: In the present study, a conducting polymer, poly[2-methoxy-5-(2-ethylhexyloxy)-1,4-phenylenevinylene] (MEH-PPV) along with a biodegradable polymer poly(ε-caprolactone) (PCL) was used to prepare an electrically conductive, biocompatible, bioactive and biodegradable nanofibrous scaffold for possible use in neural tissue engineering applications. Core-sheath electrospun nanofibres of PCL as the core and MEH-PPV as the sheath, were surface-functionalized with (3-aminopropyl) triethoxysilane (APTES) and 1,6-hexanediamine to obtain amine functionalized surface to facilitate cell-biomaterial interactions with the aim of replacing the costly biomolecules such as collagen, fibronectin, laminin and arginyl-glycyl-aspartic acid (RGD) peptide for surface modification. Scanning electron microscopy (SEM) and transmission electron microscopy (TEM) confirmed the formation of core-sheath morphology of the electrospun nanofibres, while Fourier-transform infrared spectroscopy (FTIR) and X-ray photoelectron spectroscopy (XPS) revealed successful incorporation of amine functionality after surface functionalization. Adhesion, spreading and proliferation of 3T3 fibroblast were enhanced on the surface functionalized electrospun meshes, while the neuronal model rat pheochromocytoma 12 (PC12) cells also adhered and differentiated into sympathetic neurons on these meshes. Under a constant electric field of 200 mV for 2h/day for 3 consecutive days, the PC12 cells displayed remarkable improvement in the neurite formation and outgrowth on the surface functionalized meshes that was comparable to those on the collagen coated meshes under no electrical signal. Electrical stimulation studies further demonstrated that electrically stimulated PC12 cells cultured on collagen I coated meshes yielded more and longer neurites than those of the unstimulated cells on the same scaffolds. The enhanced neurite growth and

differentiation suggest the potential use of these scaffolds for neural tissue engineering applications.

INTRODUCTION

The development of natural and synthetic nerve guidance channels (NGCs) to bridge the gap of a damaged nerve as an alternative to autologous nerve grafts in peripheral nerve repairing has been a significant research focus in recent years.[1] An ideal NGC directs the axons sprouting off the regenerating nerve end, provides a conduit for diffusion of neurotrophic factors secreted by the damaged nerve stump, and minimizes infiltrating fibrous tissue.[2] However, the engineering of such an ideal NGC with all the desired properties still remains a challenge. Concurrently, the electrical stimulation has been demonstrated to stimulate either the proliferation or differentiation of various cell types. Particularly, electroactive biomaterials such as electrets,[3] piezoelectric materials,[4,5] conducting polymers (CPs),[6-9] and more recently, carbon nanotubes (CNTs)[9,10] and graphene,[11] under the application of electrical signal, were shown to enhance the extension and regeneration of transected nerve ends indicating their potential in nerve regeneration processes.

In this regard, CPs offer excellent control over the level and duration of the electrical stimulus.[7,8] CPs have a higher charge injection limit with improved charge-discharge characteristics leading to enhanced charge transportation to cells for membrane depolarization. This, in turn, can improve the adhesion and proliferation of nerve cells including the promotion of axonal growth.[9,12] Furthermore, CP derived NGC could not only guide the axonal growth but also localize the electric stimulation as well which is generally not possible with the electrets and the piezoelectric materials.[2] Alteration of the surface charge along with surface hydrophilicity has been shown to affect the protein adsorption and the cell- iomaterial interaction, which also

make CP as an attractive candidate for a smart NGC.[2,13] It is because CPs possess inherent physical and chemical properties of organic polymers and the electrical characteristics of metals.[7,8] However, the major drawbacks associated with these CPs are difficulty in processability due to poor solubility owing to their rigid backbone, poor biodegradability and poor bioactivity due to non-permissive hydrophobic surfaces without proper recognition sites and lack of binding motifs.[14,15] Intriguingly, the electrically conducting poly[2-methoxy-5-(2-ethylhexyloxy)-1,4-phenylene vinylene] (MEH-PPV) has better solubility in common organic solvents such as chloroform, tetrahydrofuran (THF) when compared to the other CPs discussed above.[16] This advantage along with the high density of holes-traps and good biocompatibility of MEH-PPV makes it a promising candidate for tissue engineering applications[17]. Developmental work describing an optimized synthesis route for MEH-PPV electrospun composites for tissue engineering for the first time is detailed in our recent publication.[18]

With the advent of nanotechnology, the fundamental approach for fabrication of biomaterial scaffold employs electrospinning technique for the development of non-woven, three-dimensional, porous and nanofibrous scaffold with suitable mechanical properties to mimic the native extracellular matrix (ECM).[19] The simplest process involves a single fluid electrospinning of blending solutions of two or more components using a single needle, which produces monolithic fibres.[20-22] Due to poor solubility of CPs such as polyaniline (PAni), polypyrrole (PPy) and poly(3,4-ethylenedioxythiophene) (PEDOT), most of the CP based electrospun fibres were made by blending with other electrospinnable polymers in the form of monolithic fibres.[23-27] In these monolithic fibres, the CPs may or may not be homogeneously distributed, but it often compromised the conductive properties limiting its functional performances. Coaxial electrospinning, which uses two needles and solutions, one nested inside

the other, has the ability to mimic the spinneret's structure, in a single step and straight forward manner to create core-sheath nanofibres with two distinct phases and improves the functionality of the nanofibres.[28-30] For a successful coaxial electrospinning process, it was believed that the electrospinnability of the sheath polymer solution was necessary in addition to the core polymer solution. Recently, a modified coaxial electrospinning was demonstrated using an unspinnable sheath solution to create core-sheath nanofibres with uniformly distributed ultra-thin sheath layer on the core.[20-22,28-30] This modified coaxial electrospinning process doesn't only improve the functional performances of nanofibres by localizing the functional components in desired morphology but also greatly reduces the spinneret nozzle clogging problem as observed in single fluid electrospinning process. The improved functional performances of various core-sheath nanofibres using a modified electrospinning process were demonstrated for improved drug delivery and release,[20,21,28,29] and theranostic systems for magnetic resonance imaging.[22,30]

Specifically for neurite growth, numerous core-sheath nanofibres of passive polymers such as poly(lactic acid)/silk fibroin,[31] nerve growth factor (NGF) and bovine serum albumin (BSA) encapsulated poly(ε-caprolactone) (PCL) nanofibres,[32] poly(lactic-co-glycolic acid) (PLGA)/NGF,[33] etc. were reported. Although coaxial electrospinning of CPs such as PAni,[34,35] PPy,[36] PEDOT,[37,38] and MEH-PPV[16] were reported, there are almost no reports of the use of directly coaxially electrospun CP based biomaterial scaffold for neural tissue engineering except poly(L-lactic acid-co-3-caprolactone) (P(LLA-CL))/silk fibroin blend with PAni.[39] As stated above, poor solubility of CPs greatly reduces their electrospinnability. Therefore, for neural research, most of the CP based core-sheath nanofibres were prepared by coating the already electrospun nanofibres of other materials with CP through in-situ polymerization[40-43]or electrochemical deposition.[44]

Despite better solubility in common organic solvents when compared to the other CPs discussed above, direct electrospinning of MEH-PPV to uniformly distributed one-dimensional nanofibre free from bead formation is difficult. However, the good solubility of MEH-PPV provides the possibility of utilizing it as a working sheath solution for modified electrospinning process to create core-sheath nanofibres. It can be accomplished using a biocompatible, biodegradable and easily electrospinnable polymer such as PCL as the core. PCL is an aliphatic linear polyester with attractive electrospinnability due to its good rheological and viscoelastic properties.[45-48] In regard to biomedical applications, electrospun PCL scaffold has been widely studied for various tissue engineering applications owing to its biocompatibility, biodegradability and mechanical properties.[45-48]

Furthermore, the cell attachment on the biomaterial scaffold is one of the prerequisites for normal cellular functions for tissue engineering applications.[49,50] To address the poor surface hydrophilicity of CPs, their surfaces were modified with cell adhesive biomolecules such as fibronectin, laminin, collagen, RGD peptide etc. to impart bioactivity.[51,52] Unfortunately, these surface modification processes are costly and complex involving multiple conjugation steps. Therefore, an easy and inexpensive way is highly desirable to overcome these demerits, which does not need additional biomolecule treatment for cell adhesion. Surface amination may be an attractive option to achieve positively charged surface under physiological conditions and thereby, enable the biomaterial surface to interact electrostatically with the negatively charged cell surface for permitting cell adhesion.[53,54] The amino ($-NH_2$) groups on surface functionalized biomaterial also likely to interact with the carboxyl (-COOH) terminals of the integrin proteins on the cell surface through the formation of amide bonds or ionic bonds through the electrostatic attraction.[55-58]

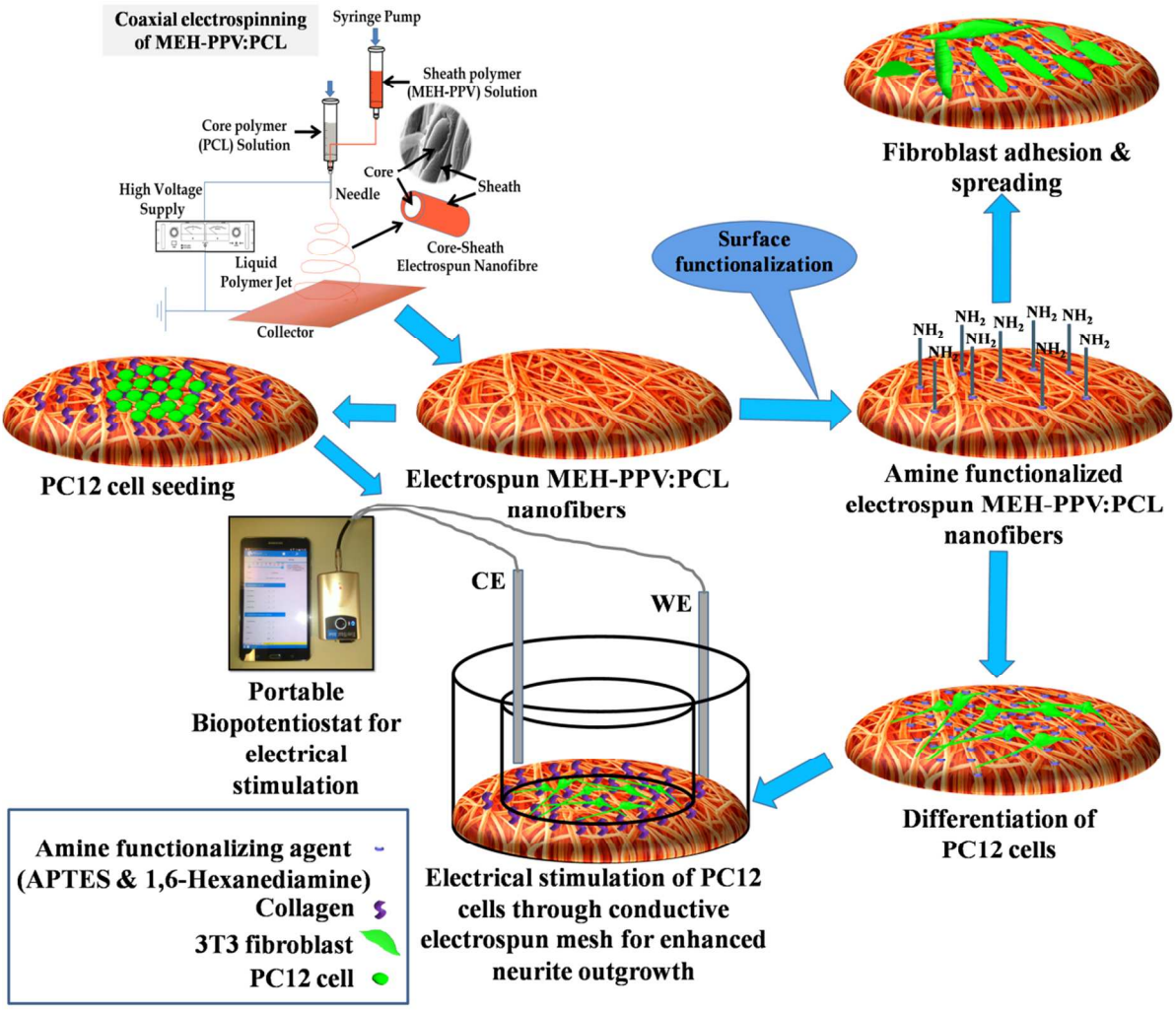

Figure 1. Schematic illustration of coaxial electrospinning of MEH-PPV:PCL nanofibres with core-sheath morphology and surface amination by APTES and 1,6-hexanediamine along with 3T3 fibroblasts adhesion and spreading and electrical stimulation of PC12 cells.

In our previous work, we optimized a synthesis route for MEH-PPV:PCL electrospun composites and shown that they support PC12 neural cell growth.[18] In the current study, we have considered the surface functionalization of the core-sheath sheath electrospun nanofibres of PCL (core) and MEH-PPV (sheath) with amine functionality to replace the need of costly biomolecules such as collagen, fibronectin, laminin; which has been eventually shown to

modulate cellular activities along with electrical stimulation. Considering the potential of amine functionality on the surface for desired cell- iomaterial interactions as mentioned above, the surface of the as-electrospun meshes has been functionalized using APTES and 1,6-hexanediamine. APTES and 1,6-hexanediamine are commonly used in biomedical applications due to their simplistic structure and minimal cost for biomolecule immobilization.[59-62] The aim of this study is to investigate the combined effect of nanofibre structure, surface functionalization and electrical stimulation through these electrospun conductive nanofibre meshes on neurite formation and neurite outgrowth. The schematic illustration of the present research flowchart is shown in **Figure 1**. If successful MEH-PPV based scaffolds could ultimately be used to design nerve guidance channels and bridge the gap between two damaged nerves.

EXPERIMENTAL DETAILS

Materials. MEH-PPV (Mw 150,000-250,000), PCL (Mw 80,000), chloroform (≥99.5%), dimethylformamide (DMF, ≥99.8%), dichloromethane (DCM, ≥99.8%), iron(III) chloride ($FeCl_3$, anhydrous, powder, ≥99.99%), APTES and 1,6-hexanediamine were procured from Sigma-Aldrich, UK and were used without further purification. Dulbecco's Modified Eagle's Medium (DMEM), fetal bovine serum (FBS), and penicillin-streptomycin (10,000 U/mL) were purchased from Gibco, UK, while trypsin–EDTA solution (Sigma-Aldrich, UK) was procured from Sigma-Aldrich, UK for NIH 3T3 cell culture. RPMI-1640 media, horse serum (Hyclone), nerve growth factor (NGF-β from rat) and collagen I (Type I solution from rat tail, BioReagent) were procured were procured from Sigma-Aldrich, UK for PC12 cell culture. CellTiter 96® AQueous One Solution Cell Proliferation Assay (MTS: [3-(4,5-dimethylthiazol-2-yl)-5-(3-carboxymethoxyphenyl)-2-(4-sulfophenyl)-2H-tetrazolium salt]) was purchased from Promega UK for the MTS assay. Primary antibody (Rb pAb to anti beta III tubulin, Abcam-ab18207),

secondary antibody (Goat pAb to Rb IgG Alexa fluor 488, Abcam-ab150077), 4',6-Diamidino-2-Phenylindole, Dihydrochloride (DAPI, Molecular Probes, UK), bovine serum albumin (BSA, Sigma-Aldrich, UK), normal goat serum (Sigma-Aldrich, UK), glycine (Acros Organics, UK), tween PBS (Pierce™ 20X PBS Tween™ 20 Buffer, Thermo Fisher Scientific, UK) were purchased for immunocytochemistry.

Analytical techniques. Morphological characterization of the electrospun nanofibres and cultured PC12 was carried out using a Zeiss SIGMA FEG-SEM (UK). Transmission electron microscopy was carried out using a TECNAI G2 20 S-TWIN (200kV); Resolution: 2.4A0, FEI COMPANY, USA, transmission electron microscope (TEM). XPS was performed using an ESCALAB 250 Xi system (Thermo Scientific, UK) equipped with a monochromated Al Kα X-ray source. Uniform charge neutralization was provided by beams of low-energy (<10 eV) Ar+ ions and low-energy electrons guided by the magnetic lens. The standard analysis spot of ca. 900×600 μm^2 was defined by the microfocused X-ray source. Full survey scans (step size 1 eV, pass energy 150 eV, dwell time 50mS and 3 scans) and narrow scans (step size 0.1 eV, pass energy 20 eV, dwell time 100 mS and 5 scans) of the C1s (BE ~285 eV) regions were acquired from three separate areas on each sample. Data were transmission function corrected and analyzed using Thermo Avantage Software (Version 5.952) with a Smart background option. FTIR spectra were recorded using a Nicolet Impact I-410 Spectrometer (SpectraLab Scientific Inc., USA). Confocal microscopy was carried out using Leica TCS SP5 Confocal Laser Scanning Microscope [CLSM] (Leica Microsystems, UK). For stability test, SEM was performed using JSM 6390LV, JEOL, Japan.

Doping of MEH-PPV. MEH-PPV was doped using $FeCl_3$ as a p-type dopant as reported by Shin Sakiyama *et al.*[63] Briefly, $FeCl_3$ was dissolved in dehydrate ethanol at a concentration of 3

mg/mL and kept stirring overnight at 50°C overnight in a laminar hood. 0.5 wt% MEH-PPV was dissolved in a 60:40 (v/v) mixture of chloroform and DMF. The dopant solution was added to MEH-PPV solution at a concentration of 2 wt% of the polymer and stirred for 30 min. The resultant solution of MEH-PPV containing dopant $FeCl_3$ was used in electrospinning.

Coaxial electrospinning of MEH-PPV:PCL. For coaxial electrospinning, PCL was dissolved in a (60:40 v/v) mixture of DCM and DMF at a concentration of 14 wt%. Both as prepared PCL solution and MEH-PPV solution were fed into two 5 mL standard plastic syringe separately attached to a coaxial spinneret. The schematic illustration and digital photograph of coaxial electrospinning are shown in **Figure S1 (a) & (b),** respectively. The flow rate was adjusted in a double-way syringe pump (KDS 200, KD Scientific Inc., USA). The coaxial spinneret with inside needle of 22 G and outside needle of 18 G was connected to a high voltage power supply (Spellman, UK). The syringe containing the core (PCL) solution was directly connected with the spinneret, while the syringe containing the sheath (MEH-PPV) solution was linked with the spinneret through an elastic silica tube of 14 G **[Figure S1 (a & b)].** The coaxial electrospinning was carried out at two flow rates of 0.6 mL/h and 1 mL/h at an applied voltage of 20 kV and a 15 cm needle tip to collector (copper plate wrapped with aluminium foil) distance. After electrospinning, the deposited meshes were air dried for overnight and carefully removed from the aluminium foil. A 77:23 v/v solution of DCM and DMF was used for electrospinning of pure PCL nanofibres at 23 kV and 2 mL/h feeding rate. Distance from needle to collector plate was 11cm. All experiments were conducted at room temperature of 18-22°C with an average humidity of 60-65%.

Surface functionalization. Electrospun meshes were surface functionalized by APTES to improve the surface hydrophilicity as reported earlier.[64] Briefly, electrospun meshes were treated

in 10 % (v/v) solution of APTES in ethanol for 18 h at room temperature. After treatment with APTES, electrospun meshes were washed with ethanol and distilled water twice to remove any unbound APTES molecules and air dried for 3 h.

The surface of the electrospun meshes was functionalized using 1,6-hexanediamine as reported elsewhere.[65] Typically, electrospun meshes were treated in 5 wt% solution of 1,6-hexanediamine in isopropanol for 3 h at 40°C. After treatment with 1,6-hexanediamine, the electrospun meshes were washed with isopropanol and distilled water twice to remove any unbound molecules and air dried for 3 h.

Stability test. To investigate the degradation and stability, all the electrospun meshes were incubated in a physiological solution of phosphate buffered saline (PBS, pH=7.4) at 37°C for 45 days as reported elsewhere.[41] Degradation and stability of the electrospun meshes were evaluated by SEM and measurements of current-voltage (I-V) characteristics after 45 days of incubation. Percentage of weight loss after 45 days has been measured using the following formula:

$$\%\ Weight\ loss = \frac{Change\ in\ weight\ after\ 45\ days\ (in\ mg)}{Original\ weight\ before\ 45\ days\ (in\ mg)} \times 100\% \qquad (1)$$

For SEM images, the samples were washed with deionized water twice to remove salts and air dried. Measurements for I-V characteristics were performed three times for each sample and surface resistivity values were determined as described above.

Sample preparation for cell culture. All electrospun meshes were cut using biopsy punch in a circular shape with diameters of 5 mm for cytotoxicity test and 10 mm for live-dead assay, immunostaining, and cell morphology study. Since PC12 cells adhere poorly to tissue culture plastic, 96 well tissue culture plate was coated with 0.01% collagen I in 0.1 M acetic acid for cytotoxicity test. Before all cell culture experiments, all electrospun meshes were kept in sterile PBS for 24 h and sterilized under UV light for 1h each side of the mesh.

Cell culture. A PC-12 (ATCC® CRL-1721™) cell line (P3) was cultured in RPMI-1640 media (Sigma-Aldrich) supplemented with 10% horse serum (Hyclone), 5% FBS (Hyclone) and 1% penicillin-streptomycin solution (Sigma-Aldrich) and were incubated at 37°C in 5% CO_2. Cells were passaged weekly using a 0.25% trypsin–EDTA solution (Sigma). The growth medium has been changed to differentiating medium containing RPMI-1640 supplemented with 1% horse serum, 1% penicillin-streptomycin solution and 100 ng/mL nerve growth factor (NGF, Sigma-Aldrich) for neuronal differentiation after 24 h of culture.

A mouse embryonic 3T3 fibroblast cell line (P15), NIH 3T3 (ATCC® CRL-1658TM) was used only for cytotoxicity study of the electrospun meshes. This cell line was cultured in Dulbecco's modified Eagle's medium (DMEM) supplemented with 10% of fetal bovine serum (FBS) and 1% penicillin-streptomycin (Pen-Strep) and were incubated at 37°C in 5% CO_2. Cells were passaged weekly using a 0.25% trypsin–EDTA solution (Sigma).

MTS proliferation assay. The MTS proliferation assay was carried out to evaluate the cytotoxicity of the electrospun meshes following incubation with 3T3 fibroblasts and PC12 cells. Metabolically active cells can reduce a tetrazolium compound into a water soluble formazan product. Non-viable cells rapidly lose their ability to reduce MTS. Therefore, the production of the coloured formazan product is proportional to the number of viable cells.[66] NIH 3T3 cells were seeded on different substrates at a concentration of 5×10^3 cells/well in a 96 well plate for the MTS assay. PC12 cells were cultured in growth medium at a concentration of 1×10^4 cells/well with direct contact with the electrospun meshes. Cell viability after 24 h incubation on the materials was quantified using CellTiter 96®AQueous One Solution containing 3-(4,5-dimethylthiazol-2-yl)-5-(3-carboxymethoxyphenyl)-2-(4-sulfophenyl)-2H-tetrazolium, inner salt), commonly known as MTS. The cultured materials were washed with sterile PBS twice, and

MTS reagent diluted 1:5 in media was added directly to all the wells except the blank. Plates were incubated for 2 h at 37°C and optical density (OD) was measured at 490 nm. All the experiments were performed at n=4.

Live/dead assay. A comparison of cell viability on the unmodified and surface modified nanocomposite films was visualized by live/dead staining of 3T3 cells using EthD-1 (staining dead cells), calcein AM (staining live cells) and DAPI (staining nucleic acid).[67] Cells were seeded at a concentration of 1×10^4 cells/well in a 48 well plate for the live/dead assay for time points of 24 h, 48 h, and 72 h. The live/dead assay was used to monitor the morphology and spreading of 3T3 fibroblasts at three different time points namely 24 h, 48 h, and 72 h so that cell behavior on unmodified and modified surfaces can be distinguished. The scaffolds seeded with 3T3 fibroblasts were washed with sterile PBS thrice prior to staining and transferred to a new culture plate. Cells were stained with a solution of 4 μM EthD-1, 2 μM calcein AM and DAPI in PBS and were then incubated for 30 min at room temperature before evaluation. Cells seeded onto the samples for the live/dead assay at the 72 h time point were used for the cell adhesion study.

Beta (III) tubulin immunochemistry. Immunocytochemistry was performed using neuronal marker beta III-tubulin to confirm the differentiation of the PC12 cells.[68] PC12 cells were cultured on uncoated and collagen I coated electrospun meshes in differentiating medium at a concentration of 1×10^5 cells/well for 6 days. Cells were washed in PBS, fixed in 100% methanol for 5 mins, washed thrice in PBS then incubated with blocking and permeabilizing solution of 1% bovine serum albumin (BSA, Sigma-Aldrich), 10% normal goat serum (Sigma-Aldrich) and 0.3 M glycine (Acros Organics) in 0.1% tween PBS for 1 h. The cells were incubated with primary antibody (Rb pAb to anti-beta III tubulin, Abcam-ab18207) at 5 μg/mL

overnight at 40°C, washed thrice in PBS then incubated with secondary antibody (Goat pAb to Rb IgG Alexa fluor 488, Abcam-ab150077) at 2 μg/mL for 1h at room temperature. The cells were stained with DAPI for nuclei counterstaining and imaged using confocal microscopy.

Cell adhesion test. SEM was performed to study the morphology and adhesion of 3T3 cells cultured on non-functionalized and functionalized electrospun meshes after 3 days. The 3T3 cells were rinsed with phosphate buffer saline (PBS) and fixed with 4% glutaraldehyde solution at 40°C for 30 min. Proliferating and differentiating morphology of PC12 cells on different electrospun meshes were evaluated using SEM after 7 days of culture. The differentiated PC12 on all the electrospun meshes were rinsed PBS and fixed with 4% glutaraldehyde solution at 40°C for 45 min. Both 3T3 and PC12 Cell seeded scaffolds were then dehydrated by incubation with serially increasing concentrations of ethanol beginning with incubation in 30% ethanol for 1 h then, 50%, 60%, 70%, 80%, 90% and absolute ethanol for 10 min each. The dehydrated cell seeded scaffolds were air dried overnight prior to SEM analysis.

Electrical stimulation of PC12 cells: Electrical stimulation of PC12 cells was performed on the collagen coated and the amine functionalized electrospun meshes according to the experimental condition as previously reported but with a slight modification.[6,12,41] The electrical stimulation experiment was set up as shown in the schematic in **Figure S3 (a) in SI**. Briefly, an Ag wire was connected to a 15 mm diameter electrospun mesh and was used as the working electrode (WE). The electrospun meshes connected to the Ag wires were fixed in a 24 well tissue culture plate. Thincert cell culture inserts (24 Well ThinCert™ Cell Culture Inserts, Greiner, New Zealand) with an inner diameter of 8.4 mm, height of 16.25 mm and working volume 0.4 mL - 1.2 mL, were fixed onto the electrospun meshes in a 24 well plate after removing the bottom membrane. The edges of the insert were sealed using poly(dimethylsiloxane) (PDMS, SYLGARD®184,

Sigma) to prevent any direct contact between the cell culture medium and the Ag wire connected to the electrospun meshes. A Pt wire placed in the cell culture medium, at a distance of 1 cm from the WE, was used as counter electrode (CE), as shown in **Figure S3 (a).** The electrospun meshes were washed thrice with sterile deionized water and incubated in sterile PBS solution overnight. The whole assembly was sterilized under UV for 3 h. PC12 cells were cultured at 1×10^3 cells/well in growth medium, and after 24 h of culture, growth medium was replaced with differentiating medium containing NGF. Then, a constant electrical potential of 500 mV/cm was applied across the electrodes for 2 h/day for 3 consecutive days using a portable bipotentiostat (EmStat Blue, PalmSens BV, Netherlands). The electrical stimulation was carried out by a double pulsed potential chronoamperometric technique in an incubator [**Figure S3 (c)**]. Current signal during electrical stimulation of PC12 cells on a random electrospun mesh was shown in **Figure S12**. The electrically stimulated PC12 cells were cultured for another 72 h without electrical stimulation. For comparison, PC12 cells on all the electrospun meshes without electrical stimulation were also cultured under the same condition for 7 days treated as control. The differentiating medium was changed every 2 days during the experimental period. All the experiments were performed n=6.

Image analysis. Confocal images of 3T3 fibroblasts cultured on different substrates acquired during live/dead assay were processed in ImageJ software for determination of viable cell density. Cell area and spreading were analyzed in ImageJ software with calcein AM stained photographs that were taken in the live/dead assay after 24 h and 48 h only. Morphological analysis was limited to the cells, which were not in physical contact with more than one cell.[69] The cells that adopted elongated, polygonal shape, with filopodia- or lamellipodia-like extensions were regarded as spreading cells.[70] In contrast, the cells that retained round

morphology were regarded as nonspreading cells. Cell spreading was evaluated in terms of percent of spreading by dividing the number of spread cells by the total number of bound cells but with round morphology. To ensure a representative count or measurement, each sample was divided into quarters and two fields per each quarter were photographed in an area of approximately 0.15 mm^2. All the experiments were repeated for six times.

The percentage of neurite bearing cells and neurite lengths were measured as reported earlier.[5,41,71,72] The number of PC12 cells on the sample meshes was determined by counting nuclei stained with DAPI dye in three fields of view (top, centre and down) for each of six repeat samples per substrate type. Neurite length was measured as a linear distance between the cell junction and the tip of a neurite. For PC12 cells, data was collected for neurite lengths at least as long as twice the diameter of the cell body. Neurite outgrowth has been reported in terms of neurite length per cell (for cells that expressed at least one neurite). Since neurite lengths were not uniformly distributed, median neurite length was also calculated. Also, the percentages of PC12 cells with neurites and the numbers of neurites per cell (for cells that expressed at least one neurite) have been calculated. In the case of neurites with an ambiguous origin, the longest neurite was retained for the measurements to prevent repeated sampling of the same neurite segment within each image.

Statistical analysis. All experiments analysis were repeated with a minimum of n = 3. Statistical analysis was performed using two-way analysis of variance (ANOVA) analysis performed. Statistically significant values were defined at α=0.05 or 0.01, whichever is applicable.

RESULTS AND DISCUSSIONS

Since MEH-PPV is soluble in a mixture of chloroform and DMF, it was utilized as sheath working solution in a modified coaxial electrospinning process to prepare highly conductive

core-sheath nanofibres with distinct homogeneous phases of PCL and MEH-PPV in the core and sheath of the nanofibres, respectively. Two different sets of bead free electrospun meshes were prepared by varying the flow rate at 0.06 mL/h and 1 mL/h. The core-sheath nanofibres electrospun at a flow rate of 0.6 mL/h and 1mL/h are denoted as CSN1 and CSN2 respectively, throughout this manuscript. CSN1 and CSN2 were surface functionalized by APTES and named as AFCSN1 and AFCSN2, respectively. Similarly, 1,6-hexanediamine functionalized CSN1 and CSN2 were denoted as HFCSN1 and HFCSN2, respectively. These six variants of the nanofibres were characterized to investigate their physico-chemical and biological properties. For PC12 cell work, CSN1 and CSN2 were coated with collagen I and named as CCSN1 and CCSN2, respectively.

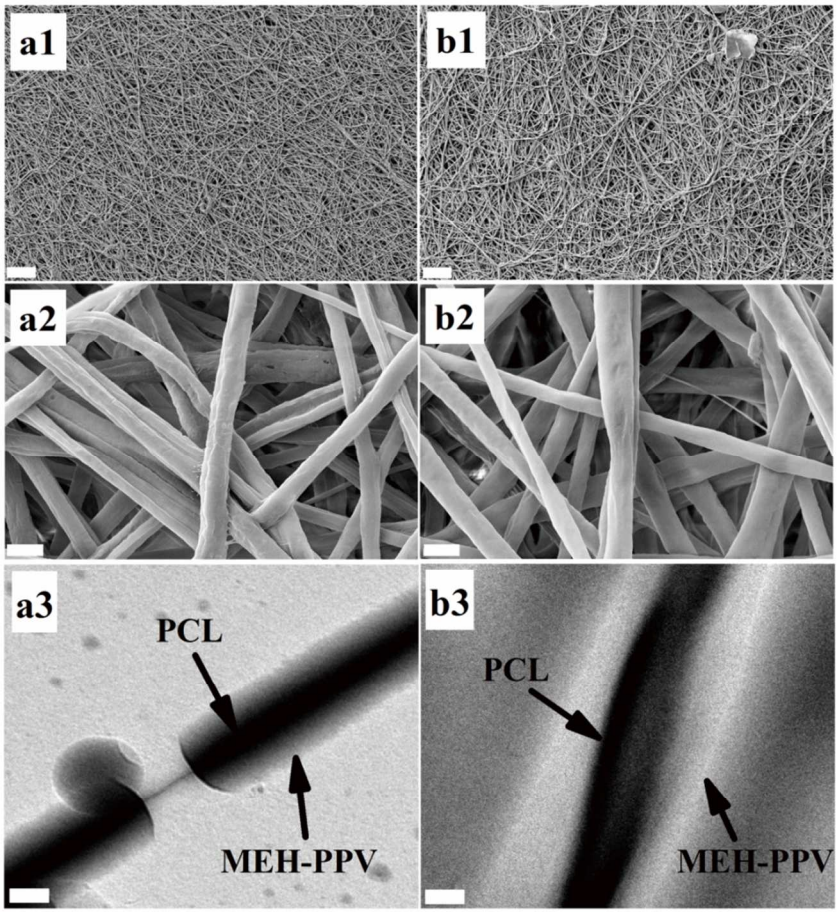

Figure 2. Scanning electron micrographs of CSN1 (a1 & a2) and CSN2 (b1 & b2), acquired at two different magnifications of 1 K and 25 K. Transmission electron micrographs of CSN1 (a3) and CSN2 (b3) showing the formation of nanofibres with core-sheath morphology. Scale bar = 20 μm (a1 & b1), 1 μm (a2 & b2) and 200 nm (a3 & b3).

Electron microscopy. The nanofibres produced by coaxial electrospinning method were found to be distributed in random directions as shown in SEM image of CSN1 [**Figure 2(a1 & a2)**] and CSN2 [**Figure 2(b1 & b2)**]. CSN1 had a median diameter of 526 ± 60 nm, whereas CSN2 had a median fibre diameter of 630 ± 137 nm as calculated from the SEM images. The diameter distributions of CSN1 & CSN2 were shown in **Figure S2 in SI**. The core-sheath morphology of CSN1 and CSN2 was confirmed by TEM [**Figure 2 (a3 & b3)**]. The sheath thickness of CSN1 and CSN2 was measured to be 158 ± 36 nm and 188 ± 52 nm, respectively, from TEM images using ImageJ software. These results are in consistent with earlier reports that higher flow rate produces nanofibres of larger diameter.[73]

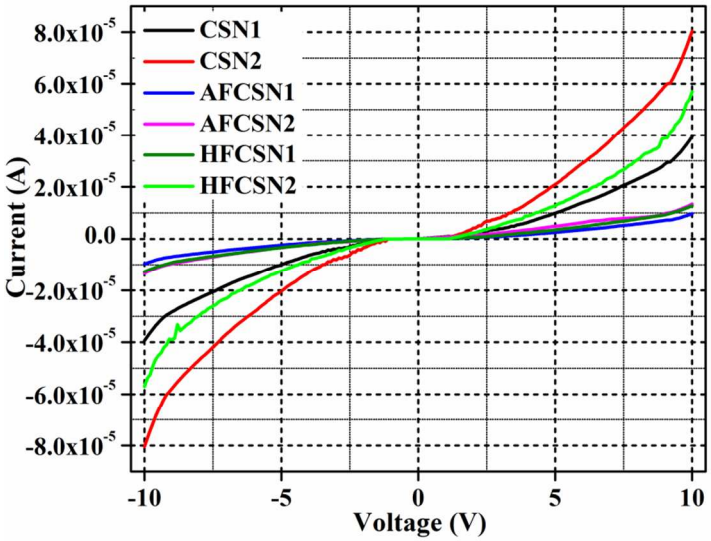

Figure 3. I-V characteristics of the core-sheath MEH-PPV:PCL nanofibres before and after surface functionalization using (a) APTES and (b) 1,6-hexanediamine at room temperature (300K).

Current-voltage (I-V) characteristics. Room temperature (300 K) I-V characteristics of the non-functionalized and surface functionalized core-sheath nanofibres were non-linear and also quite symmetric upon reversal of the voltage direction indicating possible Ohmic conduction and space charge limited conduction (SPLC) [**Figure 3**]. The surface resistivity (ρ) values (shown in Table I) of different electrospun nanofibres were calculated using the formula given below:

$$Surface\ resistivity\ (\rho) = R \times \frac{W}{D} \times t \qquad (2)$$

Where *W, D, and t* are the sample width, the distance between the two probes of the source meter and the thickness of the electrospun mesh, respectively. Surface resistance (*R)* was determined from the inverse of the slope of the I-V characteristics.

Table I. Calculated surface resistivity *(ρ)* and critical voltage *(V_c)* values of the core-sheath electrospun meshes before and after surface functionalization. Surface resistivity *(ρ)* data were expressed as Mean ± S.D (n=3).

Sample name	Surface resistivity *(ρ)* Ω.cm	Critical voltage (V_c) V
CSN1	$4.21 \pm 1.53\times10^6$	1.13
CSN2	$3.37 \pm 2.91\times10^6$	1.05
AFCSN1	$7.89 \pm 1.44\times10^6$	1.40
AFCSN2	$5.09 \pm 2.80\times10^6$	1.24
HFCSN1	$7.22 \pm 2.44\times10^6$	1.27

HFCSN2	$4.44 \pm 1.78 \times 10^6$	1.19

There was no significant change in conductive properties of the electrospun meshes after surface functionalization with APTES and 1,6-hexanediamine. Slight enhancement in surface resistivity values of the functionalized electrospun meshes was observed without any change in the nature of I-V characteristics (**Table I**). This slight increase in surface resistivity values of the functionalized electrospun meshes is attributed to the loss of pi-pi conjugation in MEH-PPV backbone during functionalization. The results demonstrated that functionalization was performed without significantly affecting the conductive properties of MEH-PPV. The electrical conduction mechanisms in these core-sheath nanofibres can be described with the help of the log-log plot of the positive side of the corresponding I-V characteristics as shown in **Figure S6 in SI**.[74] It demonstrated two distinct regions with a gradual transition between these regions: one in the lower voltage region (0<V<2) and other is in the higher voltage region (2<V<10) [**Figure S5**]. These two distinct linear regions on the log-log plot were fitted to a power law equation with different exponents, expressed as:

$$I = KV^m \qquad (3)$$

where K is a constant and m is the exponent, which can be obtained from the slope of the fitted curve. At lower voltage region, the exponent (m_1) is nearly unity and at higher voltage region, the exponent (m_2) is different from unity as shown in **Figure S6**. It indicates that at lower voltage region, the current varies linearly with voltage suggesting the charge transport mechanism is Ohmic, whereas current varies non-linearly at higher voltage region suggesting space charge limited conduction (SCLC). The observed *I-V* characteristics, with two power law regions are consistent with the space-charge limited conduction (SCLC) due to the presence of

trapped charges in MEH-PPV.[75] At low voltages, the number of injected electrons was very small as compared to the intrinsic carriers making the charge transport mechanism Ohmic. As the bias voltage was increased above 2 V, a transition from Ohmic to non-Ohmic behaviour takes place, when the density of the injected carriers became comparable to the density of the thermally generated free carriers and SCLC occurs. The critical voltage (V_c) at which the transition from Ohmic to non-Ohmic behaviour occurs can be expressed as follows:[76]

$$V_c = \frac{8}{9}\frac{qp_o d^2}{\varepsilon_o \varepsilon_r \theta} \quad (4)$$

where p_o is the density of thermally generated charge carriers, d is the sample thickness, ε_o the permittivity in free space and ε_r is the dielectric constant of the sample. The trap factor given by, $\theta = p/(p+p_t)$, where p is the density of free charge carriers and p_t is the density of trapped charge carriers, increases due to increase in the free charge carrier density (p) in the sample. The critical voltages (V_c) determined from the log-log plot from the intersection of the two linear lines extended from the linear fit as shown in **Figure S6** shifted towards lower voltage side (**Table I**). The results indicate that the lower ρ and V_c values of CSN2 than that of CSN1 and the similar trend (CSN2<CSN1<HFCSN2<AFCSN2<HFCSN1<AFCSN1) has been seen in case of their functionalized counterparts (**Table I**). The free charge carrier density (p) due to $FeCl_3$ doped MEH-PPV in the sheath contributes towards the conductive properties of the nanofibres. The lower ρ and V_c values of CSN2 that contribute towards its improved conductive behaviour, are assigned to its larger fibre diameter, which ensures higher MEH-PPV concentration in the sheath of CSN2 when compared to that of CSN1 with smaller fibre diameter. In addition, the results demonstrated that 1,6-hexanediamine functionalized nanofibres had lower values of V_c than those of their APTES functionalized counterparts (**Table I**). The

hopping of the charge carriers in the functionalized nanofibres was slightly restricted when compared to that in the non-functionalized nanofibres, suggesting the probable loss of alternating double bond conjugation in MEH-PPV during surface functionalization process. The detailed mechanisms of the non-linear behaviour of I-V characteristics of all the core-sheath nanofibres have been discussed by fitting the positive sides of the I-V data using *Kaiser Equation* in the Supporting Information [**Figure S7 & Table S2**].

Stability test. All the electrospun nanofibres were kept in PBS (pH=7.4) for 45 days to check its stability in physiological solution. The electrospun nanofibres were characterized using SEM (**Figure 4**) and the percentage of weight loss was determined after 45 days to confirm if any degradation occurred (**Table II**). There was no significant degradation of nanofibres from the SEM micrographs. The diameters of the nanofibres kept in PBS for 45 days appeared to be slightly decreased from their counterparts that were not kept in PBS (**Table II**). However, APTES functionalized meshes; i.e, AFCSN1 and AFCSN2 showed greater weight loss up to 9.09% and 7.89%, respectively than the non-functionalized (CSN1 and CSN2) and 1,6-hexanediamine functionalized (HFCSN1 and HFCSN2) meshes as shown in **Table II**. This can be attributed to the hydrolysis behavior of APTES in PBS. To study the conductive properties, the surface resistivity (ρ) values of all the nanofibres kept in PBS for 45 days, were measured. There was no significant difference between the surface resistivity of these nanofibres and their counterparts without treatment with PBS (**Table II**). The results revealed that the electrospun nanofibres were sufficiently stable in physiological solution due to nondegradable nature of MEH-PPV and slow degradation rate of PCL, which indicates the potential of these nanofibres as a conductive scaffold for tissue engineering applications, particularly for neural tissue engineering.

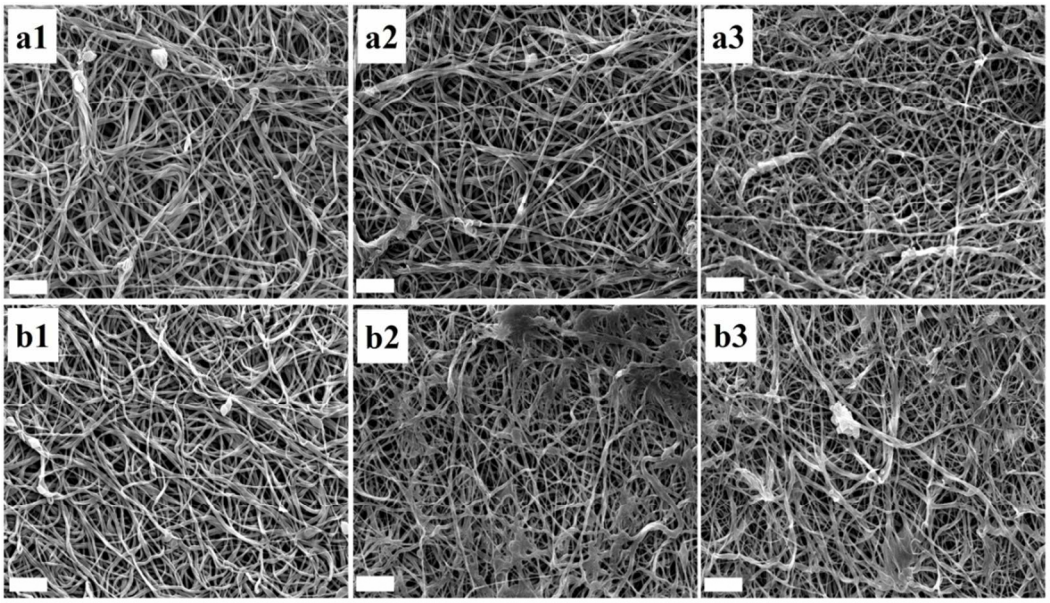

Figure 4. Scanning electron micrographs of CSN1 (a1), AFCSN1 (a2), HFCSN1 (a3), CSN2 (b1), AFCSN2 (b2) and HFCSN2 (b3), recorded after keeping in PBS (p^H=7.4) for 45 days (scale bar = 10 μm).

Table II. Fibre diameters, surface resistivity (ρ), and percentage of weight loss of the different core-sheath MEH-PPV:PCL nanofibres before and after 45 days in PBS (pH=7.4).

Sample name	Diameter (nm)		Surface resistivity (Ω.cm)		%Weight loss (After 45 days)
	Before	After	Before	After	
CSN1	546 ± 60	540 ± 192	$4.21 \pm 1.53\times10^6$	$8.98 \pm 2.21 \times 10^6$	2.45
CSN2	630 ± 137	617 ± 140	$3.37 \pm 2.91\times10^6$	$5.51 \pm 1.84 \times 10^6$	2.79
AFCSN1	531 ± 95	509 ± 118	$7.89 \pm 1.44\times10^6$	$1.89 \pm 1.32\times10^7$	9.09
AFCSN2	660 ± 151	648 ± 162	$5.09 \pm 2.80\times10^6$	$8.09 \pm 1.05\times10^6$	7.89
HFCSN1	528 ± 110	517 ± 132	$7.22 \pm 2.44\times10^6$	$9.15 \pm 1.22\times10^6$	5.12
HFCSN2	643 ± 144	637 ± 140	$4.44 \pm 1.78\times10^6$	$6.22 \pm 1.42\times10^6$	3.52

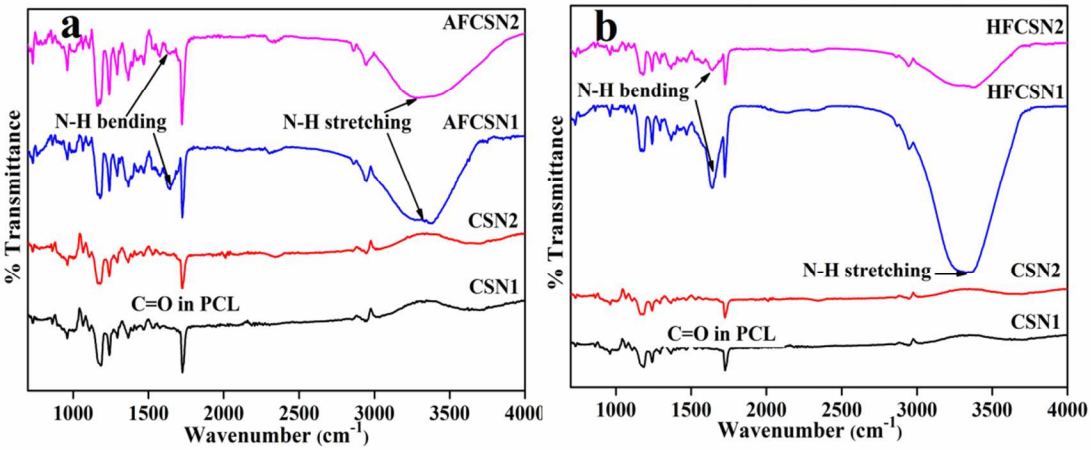

Figure 5. FTIR spectra of the core-sheath MEH-PPV:PCL nanofibres before and after surface functionalization using (a) APTES and (b) 1,6-hexanediamine.

FTIR spectroscopy. Electrospun nanofibres produced by coaxial electrospinning process showed characteristics vibrational bands for both MEH-PPV and PCL such as C=C stretch (1677 cm^{-1}), C-C ring stretch (1501-1598 cm^{-1}), aryl-alkyl ether (C-O-C) asymmetric stretch (1251 cm^{-1}) in MEH-PPV[77-79]and similarly, C=O stretching of ester groups (1723 cm^{-1}), C–O and C–C stretching (1297 cm^{-1}), O–H stretching (3500-3600 cm^{-1}) in PCL[80-82][**Figure 5**]. The FTIR spectra of pure MEH-PPV and PCL was shown in **Figure S8 in SI.** The FTIR spectra of the APTES functionalized nanofibres, exhibited several new vibrational bands including the characteristics bands of PCL and MEH-PPV as appeared in the FTIR spectra of the non-functionalized blended nanofibres **[Figure 5 (a)]**. The APTES functionalized core-sheath MEH-PPV:PCL nanofibres revealed new vibrational bands in their FTIR spectra around 1550-1567 cm^{-1} (N-H bending in secondary amine) and around 3350-3400 cm^{-1} (N-H stretching in primary amine), indicating incorporation of amine functionality on the surface of the electrospun meshes [**Figure 5 (a)**]. Besides, the characteristics band for Si-O appeared in the range 1000-1100 with significantly higher intensity, which also overlaps with the characteristics bands of PCL and

MEH-PPV.[83] The FTIR spectra of 1,6-hexanediamine functionalized nanofibres demonstrated the characteristics bands corresponding to N-H bending in secondary amine and N-H stretching in primary amine around 1550 cm^{-1} and 3400 cm^{-1}, respectively, which are not present in their non-functionalized counterparts [**Figure 5 (b)**].

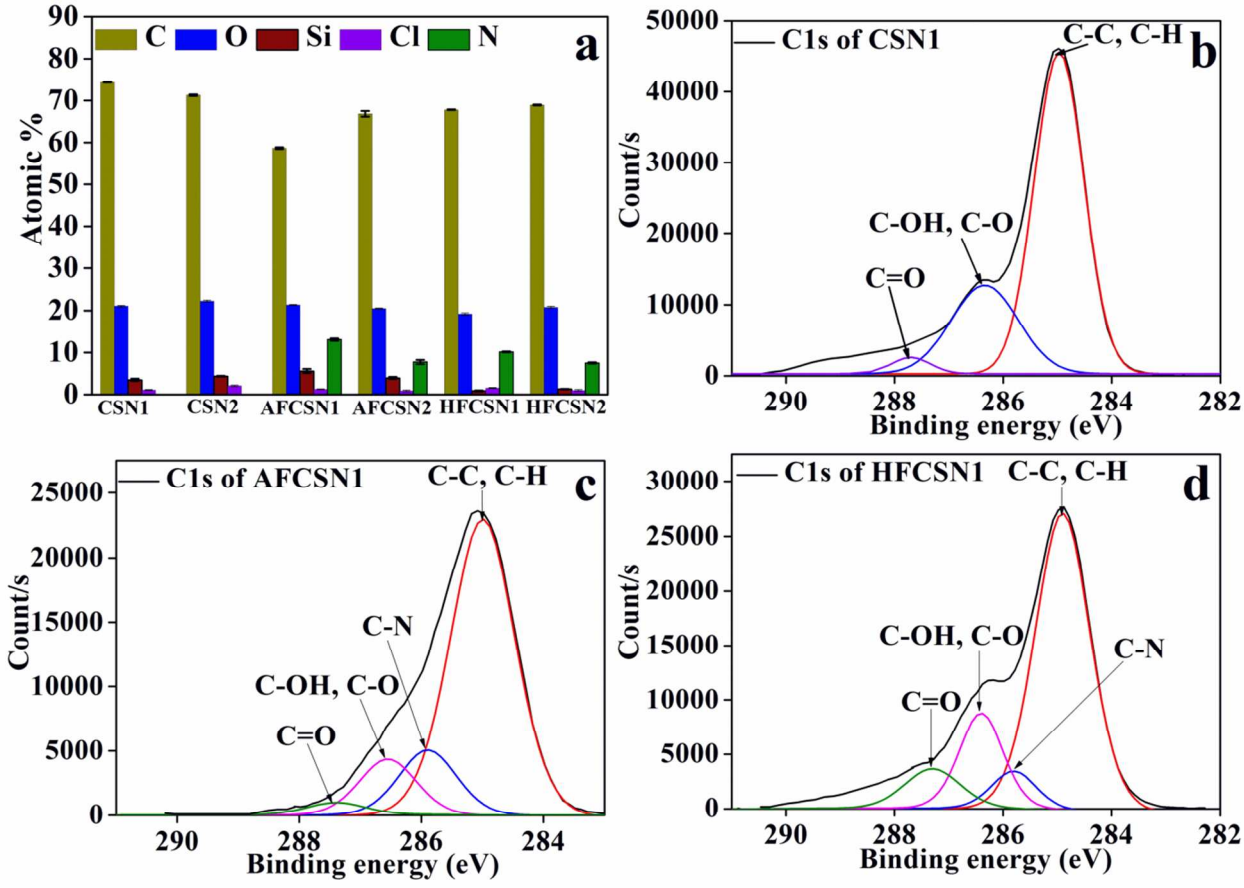

Figure 6. (a) Elemental composition in different MEH-PPV:PCL electrospun nanofibres before and after functionalization. Peak deconvolution of high-resolution C1s XPS spectra of (b) CSN1 (c) AFCSN1 and (d) HFCSN1.

Table III. Details of peak deconvolution of C1s narrow scan spectra of CSN1, AFCSN1, and HFCSN1.

Chemical group	Peak BE (eV)	Atomic % CSN1	Peak BE	Atomic % AFCSN1	Peak BE (eV)	Atomic % HFCSN1
C-C, C-H	284.99	78.59	285.01	56.63	284.94	63.25
C-N	-	-	285.91	18.95	285.76	9.65
C-OH, C-O	286.35	17.86	286.55	21.12	286.44	17.03
C=O	287.29	3.09	287.41	3.38	287.29	10.03

X-ray photoelectron spectroscopy. XPS analysis was carried out in order to understand the surface chemistry of the electrospun nanofibres and to further confirm the incorporation of amine functionality on the surface as indicated by the FTIR results. Analysis of surface elemental composition by XPS survey scans demonstrated the presence of nitrogen (N1s) on the surface of AFCSN1 (13.1%), AFCSN2 (7.79%), HFCSN1 (10.16%), and HFCSN2 (7.53%) indicating incorporation of amine functionality [**Figure 6 (a)**]. It further showed that carbon (C1s) and oxygen (O1s) were the major compositions of the electrospun nanofibres, with trace amounts of silicon (Si2p) as external contaminant **[Figure 6 (a)**]. A small amount of chlorine Cl2p was marked in CSN1 (1.1%) and CSN2 (2.1%), which indicates the doping level in MEH-PPV by $FeCl_3$. Conductive properties of the core-sheath nanofibres were not much affected after surface functionalization as trace amount of chlorine was still present in AFCSN1 (1.3%), AFCSN2 (0.9%), HFCSN1 (1.6%) and HFCSN2 (1.0%) [**Figure 6 (a)**]. The C1s core-level XPS spectra along with their peak deconvolution of CSN1, AFCSN1, and HFCSN1 are shown in **Figure 6 (b), (c) & (d)**, respectively. The details of peak deconvolution of C1s spectra of these core-sheath nanofibres are presented in **Table III**. The C1s core-level XPS spectrum of the non-functionalized CSN1 can be deconvoluted into three peak components at about 284.99, 286.35

and 287.29 eV corresponding to C-C/C-H, C-OH/C-O and C=O species, respectively [**Table III**].[84-87] The C1s core-level spectra of AFCSN1 and HFCSN1 also demonstrated the presence of these three species in addition to a new peak at about 285.91 eV for C-N species, suggesting incorporation of amine functionality on the surface of the core-sheath nanofibres after functionalization [**Table III**].[84,85] The C1s core-level XPS spectra of the core-sheath nanofibres further demonstrated that there were no XPS peak for O-C=O species corresponding to ester groups of PCL, which confirms the lone presence of MEH-PPV on the sheath of the core-sheath nanofibres.

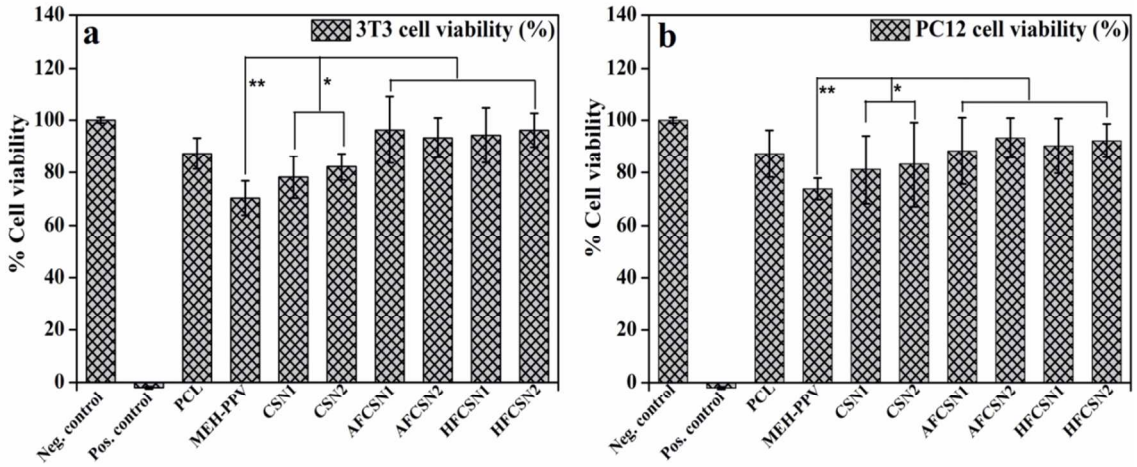

Figure 7. Percentage of cell viability in direct with different electrospun meshes after 24 h of culture . Tissue culture plastic (TCP) was used as a negative control and *tert* butyl maleate as a positive control. (a) Viability of 3T3 fibroblasts and (b) viability of PC12 cells expressed as percentage of negative control. Data were mean ± S.D, n=4. * and ** indicate statistically significant difference at $p<0.05$ and $p<0.01$, respectively.

MTS proliferation assay. Pires *et al.* reported the non-cytotoxic effect of extract of MEH-PPV with L929 fibroblasts,[88] although cytotoxicity of MEH-PPV or its composites has not been studied in direct contact with mammalian cells till our previous report.[18] MTS assay was

performed with 3T3 fibroblasts and PC12 cells in direct contact with MEH-PPV:PCL core-sheath nanofibres before and after surface functionalization including pure MEH-PPV and PCL to investigate the cytocompatibility of these materials. The MTS results shown in **Figure 7** suggest that raw MEH-PPV was less cytocompatible than MEH-PPV based electrospun meshes indicating nanofibre features might be contributing towards higher cell viability. The non-functionalized and the functionalized nanofibres demonstrated cell viability (both 3T3 and PC12 cells) 80% or above suggesting their improved biocompatibility in nanofibrous forms.[89] After surface functionalization by APTES and 1,6-hexanediamine, the core-sheath nanofibres demonstrated significantly higher 3T3 and PC12 cell viability than those on their non-functionalized counterparts at $p<0.05$ [**Figure 7 (a) & (b)**]. Moreover, the cell viability (both 3T3 and PC12 cells) on AFCSN1, AFCSN2, HFCSN1 and HFCSN2 were statistically significant from that on pure MEH-PPV at $p<0.01$ as indicated in **Figure 7 (a) & (b)**. Both 3T3 and PC12 cell viability on the functionalized nanofibres were comparable to that on the negative control (TCP) and pure PCL, while the cell viability on the non-functionalized nanofibres was statistically different at $p<0.01$ from that on the negative control (TCP) and pure PCL. It indicates the improved biocompatibility of the functionalized nanofibres due to the incorporation of the amine functionalities on the surface of the core-sheath nanofibres enabling the favorable cell-substrate interactions. Furthermore, there were no significance differences in cell viability (both 3T3 and PC12 cells) on the APTES functionalized and 1,6-hexanediamine functionalized electrospun meshes ($p=0.59$). Furthermore, the cell viability on the non-functionalized electrospun nanofibres was statistically different from that on the pure MEH-PPV at $p<0.01$. The results suggest both the nanofibre feature and surface functionalization by APTES and 1,6-

hexanediamine contributed towards the improved the biocompatibility of the electrospun nanofibres indicating their potential in tissue engineering applications.

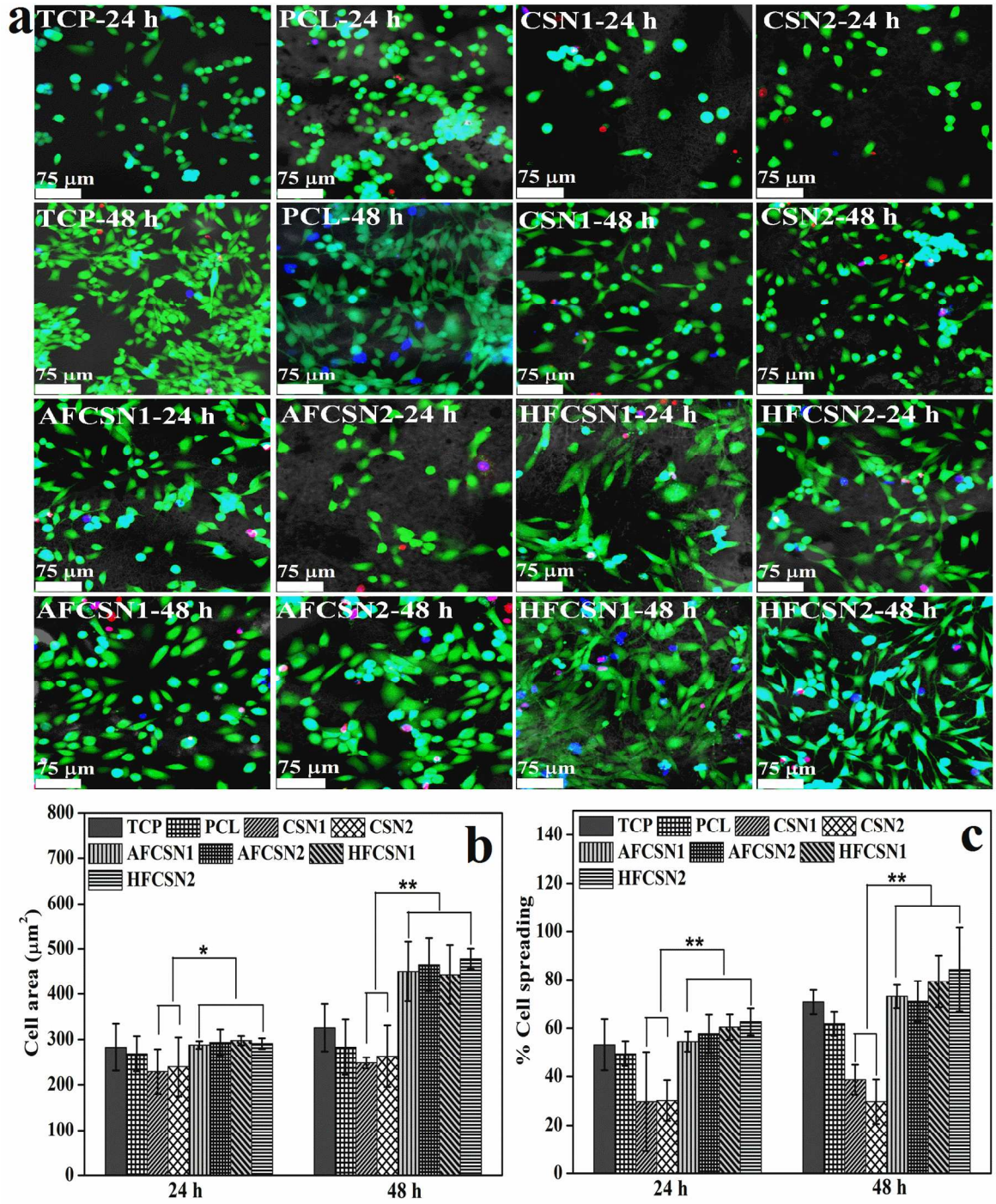

Figure 8. a. Representative confocal images with phase contrast overlay of 3T3 fibroblasts stained with calcein AM (green), EthD-1 (red) and DAPI (blue) during live/dead assay after 24

and 48 h of culture on control tissue culture plastic (TCP), electrospun PCL mesh, non-functionalized core-sheath MEH:PCL nanofibres (CSN1 and CSN2) and amine functionalized core-sheath MEH-PPV:PCL nanofibres (AFCSN1, AFCSN2, HFCSN1 and HFCSN2) as indicated. Quantitative analysis of (b) cell area (average area covered by single cell) and (c) percentage of cell spreading on various scaffolds as mentioned above. Data were presented as Mean ± S.D. * and ** indicate statistically significant difference at $p<0.05$ and $p<0.01$, respectively.

Effect of surface functionalization on 3T3 fibroblasts morphology and adhesion. Since core-sheath electrospun nanofibres alone or after surface functionalization demonstrated considerable cytocompatibility in MTS assay, it is important to study cell morphology, adhesion and spreading on those meshes to evaluate their possible use as biomaterial scaffold in tissue engineering. For that purpose, the live/dead assay was carried out to visualize the viable 3T3 fibroblasts and the changes in their morphology with time on the non-functionalized and the surface functionalized electrospun meshes. The fluorescent images of 3T3 fibroblasts cultured for 24 h and 48 h on the different scaffolds were acquired by confocal microscope after washing and staining the cells with calcein AM, EthD-1, and DAPI. Representative confocal images are shown in **Figure 8 (a)** as labeled. The green-fluorescent calcein can be visualized throughout almost all of the cell bodies seeded on different scaffolds indicating the viable cells, except few dead cells (red) **[Figure 8 (a)]**. This again confirmed the cytocompatibility of these electrospun meshes. The cells were also stained with DAPI for nuclei staining; however, only a few DAPI stained nuclei (blue) can be seen. This might be because of the staining of the cells without fixing. It is evident from the confocal images that the cells seeded on surface functionalized electrospun meshes adopted more spreading morphology, i.e., a flattened, polygonal or elongated

shape. To determine the effect of surface functionalization on different cellular activities, cell density, projected cell area and percentage of cell spreading were quantified using the confocal images of 3T3 fibroblasts seeded on different scaffolds. Cells seeded on TCP and electrospun PCL nanofibres were also analyzed and treated as control.

Two-way ANOVA analysis indicateed that the 3T3 cell density, after 24 h and 48 h of culture, on AFCSN1 (109±23 and 133±25), AFCSN2 (87±15 and 160±15), HFCSN1 (98±20 and 156±17) and HFCSN2 (107±26 and 177±27) statistically differed from that on the non-functionalized CSN1 (61±16 and 109±29) and CSN2 (53±11 and 103±21) at $p<0.05$ [**Figure S11**]. However, cell density on the controls (TCP and PCL) were not significantly different from that on the surface functionalized electrospun meshes at the both time points. Quantitative analysis using two-way ANOVA anlysis demonstrated that the projected cell area and the percent of cell spreading after 24 h and 48 h of culture on the surface functionalized electrospun meshes were higher than that on the non-functionalized electrospun meshes [**Figure 8 (b) & (c)**]**.** The differences in the projected cell area were statistically significant at $p<0.05$ and $p<0.01$ at 24 h and 48 h, respectively [**Figure 8 (b)**], while the the percnt of cell spreading is significantly different at $p<0.01$ at the both time points [**Figure 8 (c)**]. The statistical analysis to determine the sample type effect on the projected cell area demonstrated no significance differences on the APTES functionalized meshes (AFCSN1 & AFCSN2) and the 1,6-hexanediamine functionalized meshes (HFCSN1 & HFCSN2). Interstingly, the area covered by each cell on the surface functionalized meshes is statiscally different at $p<0.01$ from the controls (TCP & PCL) after 48 h, whereas there was statistical difference after 24 h. Similarly, the extent of cell spreading on the surface functionalized meshes was higher than that on the controls (TCP & PCL) and the differences were statistically significant at $p<0.05$ at the both time points. Unlike the projected

cell area, the extent of cell spreading on the 1,6-hexanediamine functionalized meshes was statistically different at $p<0.05$ from that on the APTES functionalized meshes after 24 and 48 h. Nonetheless, the differences in the cell density, the projected cell area and the cell spreading on CSN1 and CSN2, including their functionalized counterparts were not significant.

The results suggest the enhanced 3T3 fibroblast adhesion, spreading and proliferation on the surface functionalized electrospun meshes is attributed to the incorporation of amine functionality, leading to induce favorable interaction with the receptor proteins on the cell surface.[90,92] Concurrently, 1,6-hexanediamine functionalized electropsun meshes demonstrated enhanced cellular activities such as projected cell area and cell apreading than those on the APTES functionalized electropsun meshes. This observation is supported by the evidence of the higher amount of amine functionality on the surface of the electrospun meshes after functionalization by 1,6-hexanediamine as shown by XPS results. However, no significant effect of fibre diameter on cell adhesion and morphology was oberved in the present study.

To further confirm the results described above, the 3T3 cells cultured for 3 days on the electrospun meshes were characterized by SEM and shown in **Figure 10**. SEM images revealed that 3T3 cells adhered and spread well on AFCSN1 [**Figure 9 (c)**], AFCSN2 [**Figure 9 (d)**], HFCSN1 [**Figure 9 (e)**] and HFCSN2 [**Figure 9 (f)**] as compared to the non-functionalized CSN1 [**Figure 10 (a)**] and CSN2 [**Figure 9 (b)**]. Although the nanofibres were randomly oriented, the cells were aligned in some particular directions on the surface functionalized meshes with simultaneous formations of filopodia and lamellipodia-like extensions, which are pointed with the help of red, yellow and orange arrows in the insets of **Figure 9 (a)-(f)**. This observation indicates that the cells on surface functionalized meshes interacted well with the surrounding fibres and started to migrate through the porous nanofibrous network. The amine

functionality on the surface functionalized meshes provides necessary binding sites to the integrin proteins on the cell surface resulting in the formation of focal adhesions; which are confirmed from the appearance of filopodia and lamellipodia-like extensions [Insets of **Figure 9 (c)-(f)**]. This accelerates the cell attachment, followed by cell spreading and migration. In contrast, the non-functionalized meshes due to lack of bioactive binding sites showed poor cell attachment and morphology when compared to the surface functionalized meshes [**Figure 9 (a) & (b)**]. The observed cell attachment on the non-functionalized meshes may be due to the serum proteins adsorbed by the fibres, which offer limited focal adhesions for cell attachment.[94] These results further revealed that cells cultured on the 1,6-hexanediamine functionalized electrospun meshes i.e., HFCSN1 and HFCSN2 appeared to be bigger in size and adopted more elongated morphology than that on the APTES functionalized electrospun meshes, i.e., AFCSN1 and AFCSN2, which is in agreement with quantitative analysis of live/dead confocal images. These results suggest that surface functionalized electrospun meshes provide a bioactive three-dimensional nanofibrous structure for fibroblast attachment, growth, and migration through contact guidance phenomenon.[93]

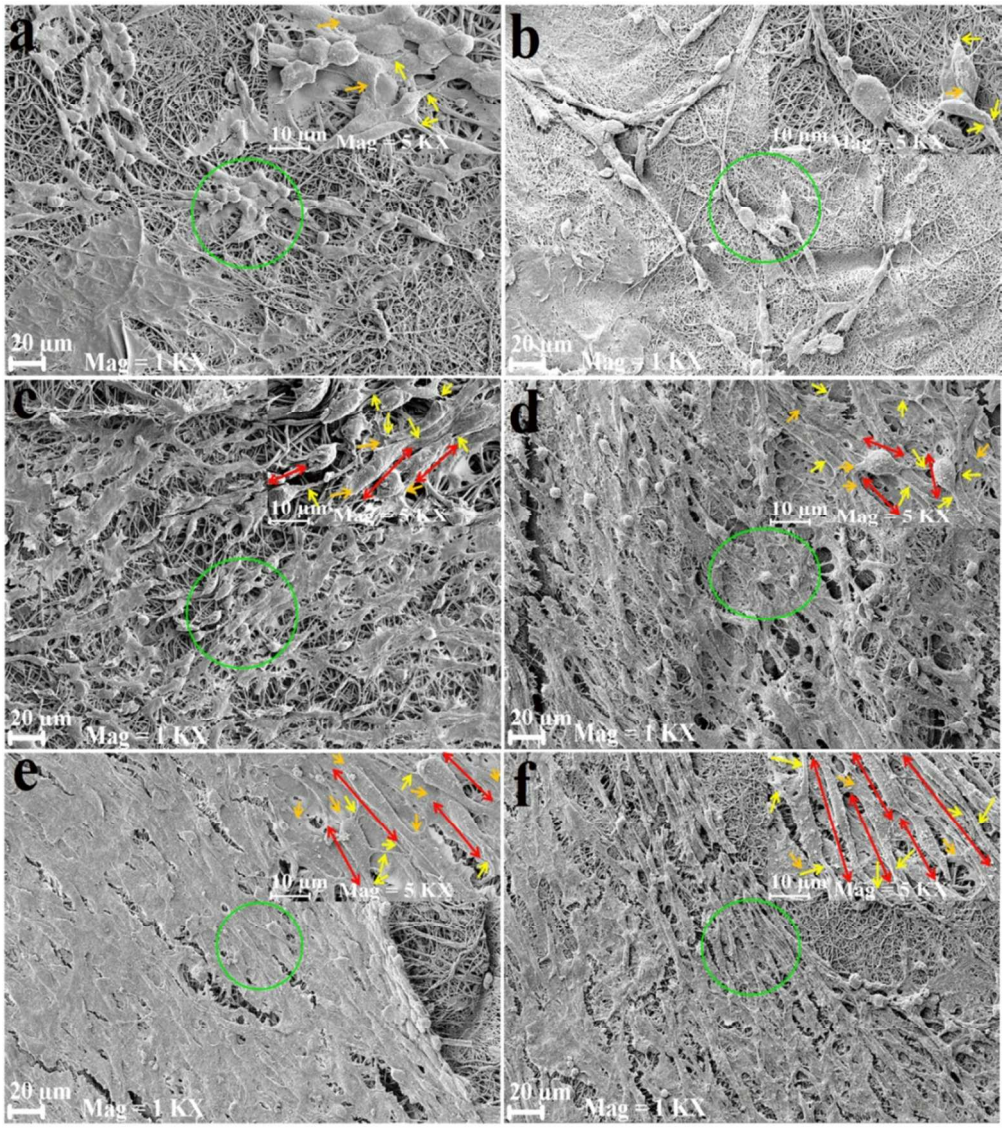

Figure 9. Scanning electron micrographs of 3T3 fibroblasts after 3 days culture on CSN1 (a), CSN2 (b), AFCSN1 (c), AFCSN2 (d), HFCSN1 (e) and HFCSN2 (f). Insets of (a)-(f) show magnified image of green circled region. Red, yellow and orange arrows indicate the direction of cell alignment, filopodia- and lamellipodia-like extensions, respectively.

Figure 10. Immunolabelling of beta (III) tubulin in differentiated PC12 cells with DAPI stained nuclei after 7 days of culture on CSN1 (a1), CSN2 (b1), AFCSN1 (a2), AFCSN2 (b2), HFCSN1 (a3), HFCSN2 (b3), CCSN1 (a4) and CCSN2 (b4). White arrows show neuronal cell bodies with at least one neurite formed. Red arrows represent neurons with long branched neurites and/or growth cones. Percentage of neurite-bearing cells (c) and neurite length per cell (d) on different electrospun meshes along with collagen-coated glass presented as Mean ± S.D. Insets of (c) and (d) show immunostained PC12 cells cultured on controls for 7 days, i.e., collagen-coated cover slip and collagen coated electrospun pure PCL mesh, respectively. * and ** indicate statistically significant difference from non-functionalized CSN1 and CSN2 at $p<0.05$and $p<0.01$, respectively.

Effect of surface functionalization on PC12 cell adhesion and differentiation. The PC12 cells, derived from a rat pheochromocytoma, were cultured for 7 days in differentiating medium on different electrospun MEH-PPV: PCL meshes without and in conjunction with collagen I coating to investigate the suitability of these materials for neuronal applications. This cell line has been widely used as a model neuronal system. PC12 cells cultured with NGF develop long neurite outgrowth, become electrically excitable and take on many of the biochemical traits of sympathetic noradrenergic neurons.[94] Since, PC12 cells readily adhere to collagen, pristine electrospun meshes were also coated with collagen I. Collagen I is a fibril-forming collagen present in ECM of peripheral nervous system (PNS) and play an important part in the development of the peripheral nervous system as well as in the maintenance of normal peripheral nerve function during adulthood.[95] The PC12 neuronal differentiation was studied on these collagen coated meshes along with the APTES and 1,6-hexanediamine functionalized meshes in

order to compare the effectiveness of surface functionalization towards supporting the PC12 differentiation. Immunolabelling with beta (III) tubulin antibody was performed to confirm the PC12 cell differentiation to sympathetic neurons. The PC12 cells grown on the uncoated and collagen coated electrospun meshes were labeled with beta (III) tubulin antibody to visualize cytoskeletal microtubules, which are dynamic polymer filaments of alpha and beta tubulin subunits that drive neurite outgrowth and control neuronal morphology.[71]

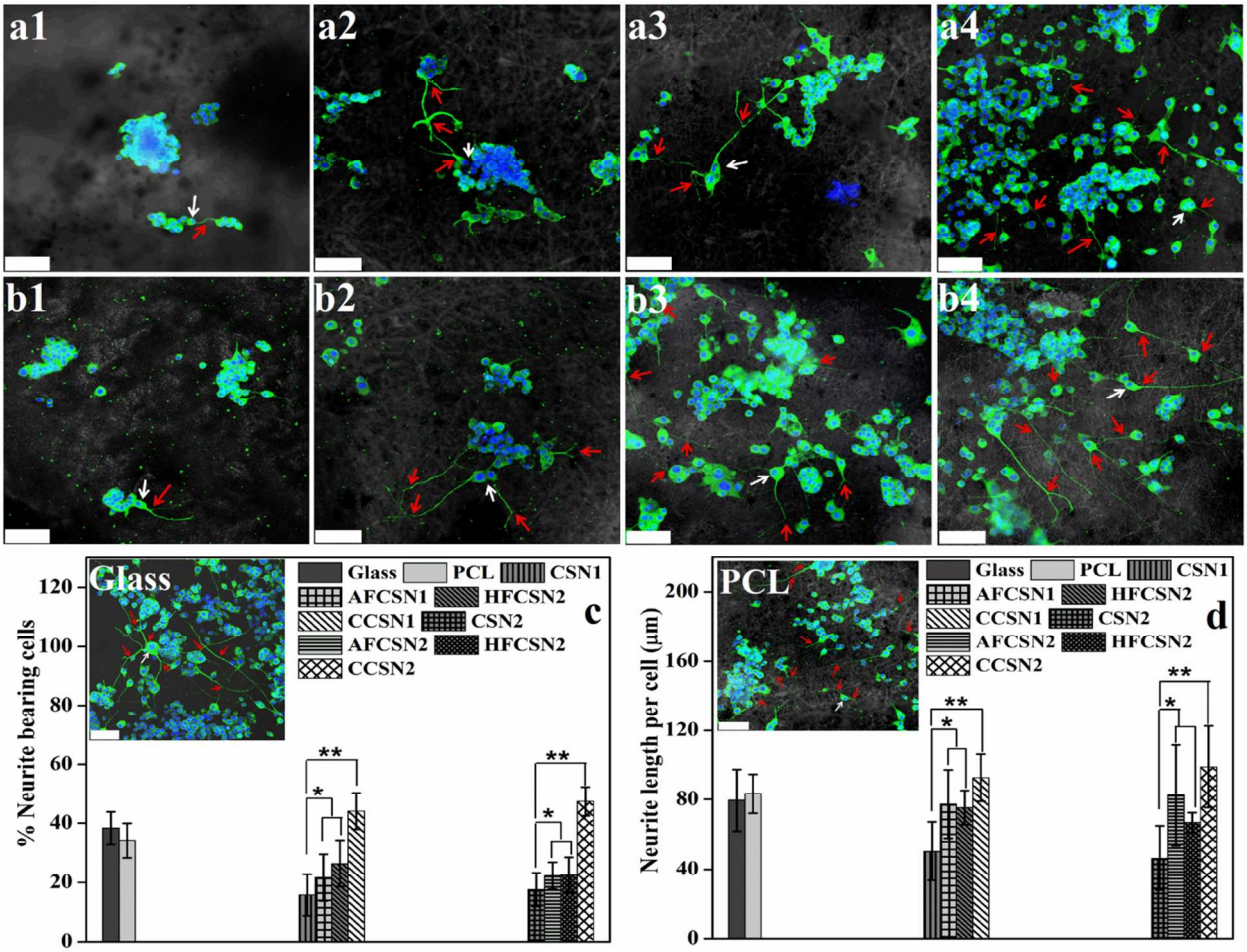

Figure 10. Immunolabelling of beta (III) tubulin in differentiated PC12 cells with DAPI stained nuclei after 7 days of culture on CSN1 (a1), CSN2 (b1), AFCSN1 (a2), AFCSN2 (b2), HFCSN1 (a3), HFCSN2 (b3), CCSN1 (a4) and CCSN2 (b4). White arrows show neuronal cell bodies with

at least one neurite formed. Red arrows represent neurons with long branched neurites and/or growth cones. Percentage of neurite-bearing cells (c) and neurite length per cell (d) on different electrospun meshes along with collagen-coated glass presented as Mean ± S.D. Insets of (c) and (d) show immunostained PC12 cells cultured on controls for 7 days, i.e., collagen-coated cover slip and collagen coated electrospun pure PCL mesh, respectively. * and ** indicate statistically significant difference from non-functionalized CSN1 and CSN2 at $p<0.05$and $p<0.01$, respectively.

The beta (III) tubulin staining was visualized all through the cell bodies and neurites formed on the collagen coated (CCSN1 & CCSN2) and the surface functionalized electrospun meshes (AFCSN1, AFCSN2, HFCSN1 & HFCSN2) [**Figure 10**], which confirmed the neural differentiation of the PC12 cells on these scaffolds. Beta (III) tubulin labeling displayed the consistent neuronal morphology for the differentiated PC12 cells on all the coated electrospun meshes **[Figure 10 (a4 & b4)]** as compared to the uncoated electrospun meshes. The majority of the differentiated PC12 cells on the coated electrospun meshes demonstrated neuronal characteristics with long neurites with or without branches of varying complexity, round somas of variable size and many growth cones **[Figure 10 (a4 & b4)]**. The uncoated but APTES functionalized meshes **[Figure 10 (a2 & b2)]** and 1,6-hexanedimaine functionalized meshes **[Figure 10 (a3 & b3)]** also supported the neuronal differentiation of PC12 cells, however, the extent of neurite formation, outgrowth or branching was not consistent when compared to that on the collagen coated meshes or the controls: collagen coated glass cover slip [Inset of **Figure 10 (c)**] and electrospun pure PCL mesh [Inset of **Figure 10 (d)**]. In contrast, PC12 cells on the uncoated and non-functionalized meshes formed clusters with very poor & short or no neurite formation with few or no branches and growth cones **[Figure 10 (a1 & b1)].** This can be

assigned to the poor cell attachment on the uncoated and non-functionalized meshes. Quantitative analysis of beta (III) tubulin immunochemistry results using ImageJ software revealed the poor cell attachment on the uncoated and non-functionalized CSN1 (39 ± 16 per image) and CSN2 (40 ± 11 per image) when compared to AFCSN1 (94 ± 18 per image), AFCSN2 (82 ± 15 per image), HFCSN1 (94 ± 12 per image), HFCSN2 (91 ± 17 per image), CCSN1 (188 ± 24 per image) and CCSN2 (198 ± 29 per image). Thus, the surface functionalized electrospun meshes demonstrated better cell attachment than that on the pristine (non-functionalized and not coated with collagen I) meshes and the difference was found to be statistically significant at $p<0.05$ from two-way ANOVA analysis. The difference of cell attachment on the collagen-coated electrospun meshes was also statistically significant at $p<0.01$ from that on the pristine meshes indicating their potential for neural tissue engineering applications. At least 600 cells and 350 neurites were analyzed for quantitative analysis of neurite formation and neurite outgrowth. Due to poor attachment of PC12 cells on the non-functionalized electrospun meshes, the number of cells analyzed was not more than 150-200 per substrate and accordingly, the number of neurites is below 100 only.

The percentage of cells that formed neurite and neurite length per cell (for cells that possess at least one neurite) on CCSN1 (44 ± 6% and 92 ± 11 μm, N=811, m=521) and CCSN2 (47 ± 5% and 98 ± 22 μm, N=845, m=498) were significantly higher than those on pristine CSN1 (15 ± 7% and 49 ± 14% μm, N=231, m=85) and CSN2 (17 ± 6% and 45 ± 15 μm, N=251, m=91), at $p<0.01$, where 'N' and 'm' are number of cells and number of neurites analysed, respectively [**Figure 10 (c) & (d)**]. Similarly, the differentiated PC12 cells formed more and longer neurites on AFCSN1 (22 ± 8% and 79 ± 17 μm, N=609, m=397), AFCSN2 (23 ± 6% and 84 ± 24 μm, N=623, m=389), HFCSN1 (28 ± 7% and 77 ± 12 μm, N=644, m=417)

and HFCSN2 (24 ± 5% and 75 ± 7 μm, N=619, m=412) than those on their non-functionalized counterparts [**Figure 10 (c) & (d)**] and there exists statistical significance at $p<0.05$. Furthermore, the percentage of neurite bearing cells and the neurite outgrowth on the collagen coated meshes were higher than those on the surface functionalized meshes, which is statistically significant at $p<0.05$. Nonetheless, the cellular activity of PC12 cells was not significantly different on the APTES and the 1,6-hexanediamine functionalized meshes. It seems that surface functionalization by both the functionalizing agents contributes equally towards the PC12 attachment and their neural differentiation in presence of NGF. The overall observations suggest that both APTES and 1,6-hexanediamine functionalized meshes provided more PC12 cell attachment and their differentiation to sympathetic neurons than pristine meshes. The better PC12 attachment followed by their cellular activities like neurite formation and outgrowth on the surface functionalized meshes can be attributed to the incorporation of amine functionality on their surfaces enabling them to achieve favorable electrostatic interactions with negatively charged cell surfaces or to interact through amide bond formation between amino groups on the surface with the carboxyl terminus of integrin proteins on the cells surface for cellular adhesion and differentiation.[55-58,96,97] These results further revealed that fibre features along with collagen coating on scaffold provide a better platform for neurite formation and neurite outgrowth since PC12 cells formed more neurites with longer outgrowth on collagen-coated electrospun meshes than those on collagen-coated glass ($p<0.01$). It has been also noted that MEH-PPV in the sheath of the core-sheath nanofibres did not have any adverse effect on neurite formation and outgrowth, which is in agreement with the MTS and live/dead results. CCSN1 and CCSN2 revealed the greater number of neurite bearing cells and the longer neurite growth on them than those on the collagen coated control glass cover slip and electrospun pure PCL mesh, which are

statistically significant at $p<0.01$. It is occurred that the cell to cell contact and cell signaling on the electrically conducting CCSN1 and CCSN2 are more pronounced, which was reported to initiate the Ca^{2+} signal conduction, an indirect indicator of action potential.[5,98] Thus, the electrically conductive property of the core-sheath nanofibres in conjunction with collagen, ultimately are believed to induce better neural differentiation of PC12 cells and neurite outgrowth on CCSN1 and CCSN2.

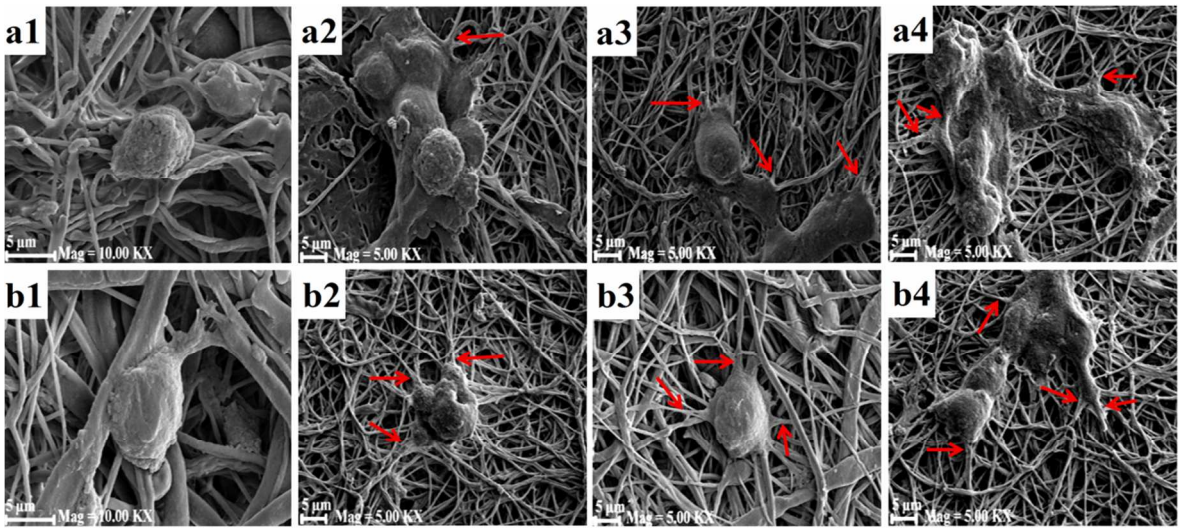

Figure 11. Scanning electron micrographs of PC12 cells after 7 days cultured on pristine CSN1 (a1), AFCSN1 (a2), HFCSN1 (a3), CCSN1 (a4), CSN2 (b1), AFCSN2 (b2), HFCSN2 (b3), and CCSN2 (b4). Red arrows show neurite projections on different electrospun meshes.

To further confirm the attachment of PC12 cells and to study its morphology on the various electrospun meshes, SEM was performed after 7 days of culture. SEM images confirmed improved cell attachment on the collagen-coated electrospun meshes than the surface functionalized meshes, whilst poor cell attachment on the pristine electrospun meshes. All the electrospun meshes coated with collagen I showed significantly better cell adhesion and morphology than that on the non-functionalized electrospun meshes. PC12 cells on the coated

electrospun meshes appeared to make contact with multiple fibres and formed more elliptical morphologies with neurite projection [**Figure 11 (a4 & b4)**]. The cells on the uncoated electrospun meshes were seemed to be spherical [**Figure 11 (a1 & b1)**] with distorted morphology and with few or no neurite projections. However, better PC12 morphology, attachment, and neurite projections were observed on the both amine functionalized meshes [**Figure 11 (a2, b2, a3 & b3)**]. Although not quantified, it was also worthy to be noted that PC12 cells cultured on the surface functionalized meshes were bigger in size than that of cultured on the pristine and the collagen-coated meshes. The results confirmed good cell attachment on the collagen-coated electrospun meshes along with good neurite projections in random directions indicating the potential of the coated electrospun meshes for neural tissue engineering applications. The moderate enhancement in PC12 attachment and neurite projections on surface functionalized conductive meshes also indicated the potential of these meshes for nerve repair.

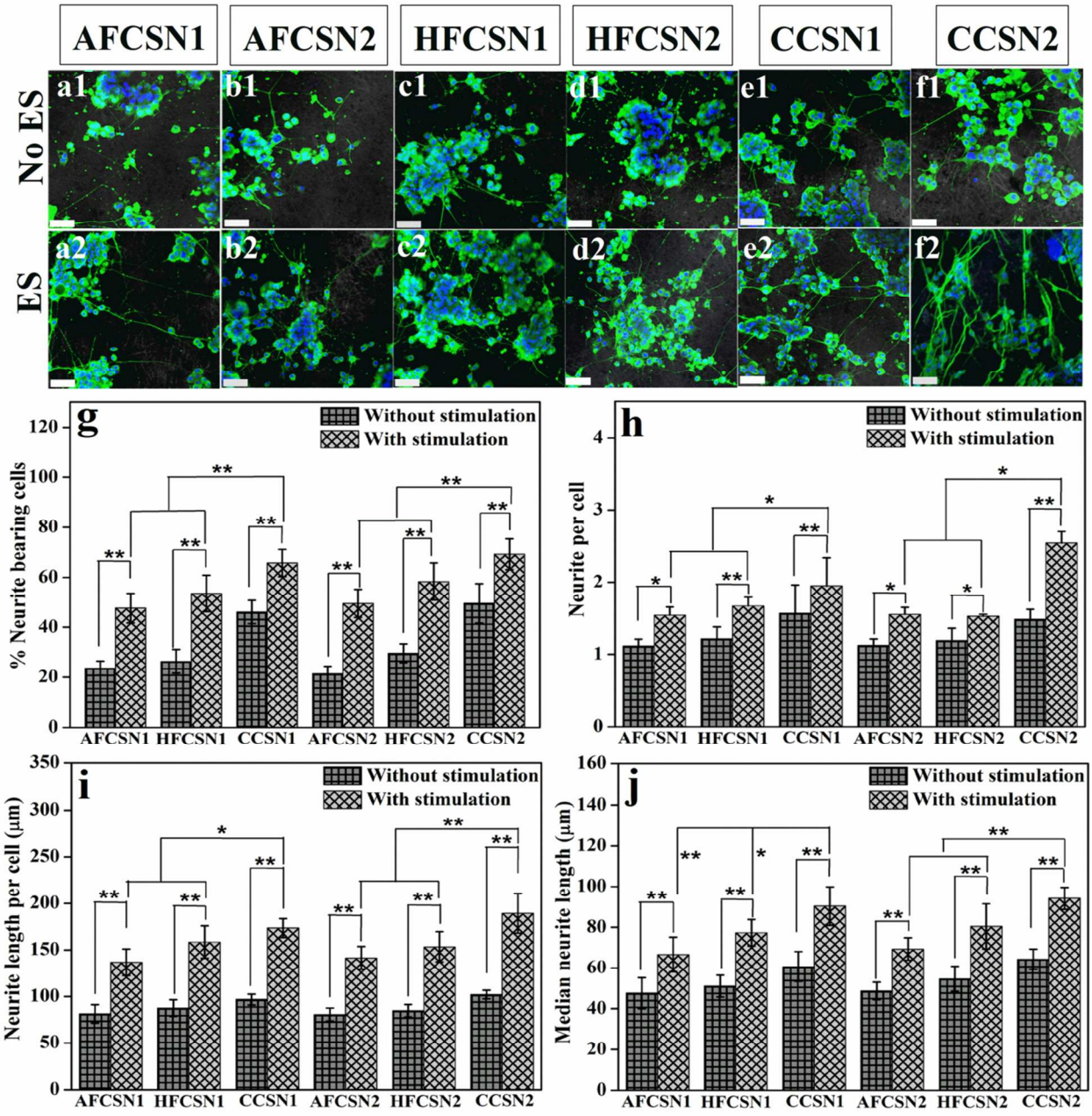

Figure 12. Confocal images with phase contrast overlay of beta (III) tubulin immunostained PC12 cells cultured for 7 days on the various core-sheath electrospun meshes under no electrical stimulation (a1-AFCSN1, b1-ACSN2, c1-HFCSN1, d1-HFCSN2, e1-CCSN1, f1-CCSN2) and under electrical stimulation of 500 mV/cm for 2h/day (a2-AFCSN1, b2-AFCSN2, c2-HFCSN1,

d2-HFCSN2, e2-CCSN1, f2-CCSN2) [Scale bar = 75 μm]. (g) percentage of neurite bearing cells, (h) neurite per cell, (i) neurite length per cell and (j) median neurite length of differentiated PC12 cells on the various core-sheath MEH-PPV:PCL electrospun meshes without electrical stimulation and with electrical stimulation. Data were Mean ± S.D. * and ** indicate statistically significant difference at $p<0.05$ and $p<0.01$, respectively (n=6).

Electrical stimulation of PC12 cells. To explore the potential of the different amine functionalized and collagen-coated electrospun meshes for electrical stimulation of nerve cells as smart biomaterial scaffolds for axonal regeneration in damaged nerve, electrical stimulation of PC12 cells was accomplished in differentiating medium as shown in the schematic in **Figure S3**. PC12 cells were also cultured on electrospun meshes in the homemade electrical stimulation set up without electrical stimulation for comparison. The results indicated that the presence of electrically conductive MEH-PPV in the sheath of the nanofibres increases the percentage of neurite bearing cells and the neurite extension following 2 h growth under electrical stimulation. The healthy neuronal characteristics including greater neurite formation, branching, and longer axonal growth were observed on the electrically stimulated cells [Figure 12 (a2-f2)] when compared to the unstimulated cells **[Figure 12 (a1-f1)]**. The APTES and 1,6-hexanediamine functionalized electrospun meshes, which demonstrated lower neurite formation and outgrowth under no electrical stimulation **[Figure 12 (a1-e1)]**, displayed remarkable enhancement in the neurite formation and outgrowth under 2h of electrical stimulation at 500 mV/cm per day for three consecutive days **[Figure 12 (a2-e2)]**. The effectiveness of electrical stimulation on neuronal growth of the PC12 cells was assessed through the quantitative analysis of the confocal images of beta (III) tubulin stained cells using ImageJ software and was discussed below.

Quantitative analysis indicated that enhanced neurite formation on electrically stimulated PC12 cells on AFCSN1 (48 ± 6%, N=576, m=301), AFCSN2 (50 ± 6%, N=587, m=323), HFCSN1 (54 ± 7%, N=607, m=386), HFCSN2 (58 ± 8%, N=628, m=422), CCSN1 (66 ± 6%, N=655, m=678) and CCSN2 (70 ± 6%, N=702, m=658) than that on unstimulated PC12 cells on AFCSN1 (24 ± 4%, N=504, m=265), AFCSN2 (21 ± 3%, N=484, m=234), HFCSN1 (26 ± 5%, N=530, m=291), HFCSN2 (29 ± 4%, N=544, m=301), CCSN1 (46 ± 5%, N=674, m=501) and CCSN2 (50 ± 8%, N=692, m=476), where 'N' and 'm' denote number of cells and number of neurites analyzed [**Figure 12 (g)**]. These differences were statistically significant at $p<0.01$ as revealed by two-way ANOVA analysis with replication [**Figure 12 (g)**]. This observation was further evident from the fact that the PC12 cells under electrical stimulation form more neurites per cell than that formed per unstimulated cells. Analysis of neurites per cell indicated that single stimulated cell had 1.51 (AFCSN1), 1.56 (AFCSN2), 1.65 (HFCSN1), 1.53 (HFCSN2), 1.98 (CCSN1), and 2.56 (CCSN2) neurites on average as compared to 1.11 (AFCSN1), 1.12 (AFCSN2), 1.2 (HFCSN1), 1.19 (HFCSN2), 1.57 (CCSN1) and 1.48 (CCSN2) neurites per unstimulated cells [**Figure 12 (h)**]. However, the number of neurites per stimulated cell was found to be statistically different for HFCSN1, CCSN1 and CCSN2 at $p<0.01$, while it was statistically significant at $p<0.05$ for AFCSN1, AFCSN2 and HFCSN2 from that of the unstimulated cells [**Figure 12 (h)**]. Turning on to the evaluation of the effect of sample type on neurite formation under electrical stimulation, the results indicated no consistent significance difference in the percentage of neurite bearing cells and neurite per cell between CCSN1 and CCSN2 including their functionalized counterparts. Nonetheless, it was found that the percentage of neurite bearing cells under electrical stimulation was significantly different on the collagen coated meshes from that on the surface functionalized meshes at $p<0.01$ [**Figure 12**

(g)], while the neurite per cell was statistically different at $p<0.05$ on the collagen coated meshes and the surface functionalized meshes [**Figure 12 (h)**].

Quantitative analysis to determine the effect of electric field on axonal growth revealed that the neurite lengths per cell and median neurite lengths of electrically stimulated cells were more on AFCSN1 (136 ± 15 and 66 ± 10 μm), AFCSN2 (141 ± 12 and 69 ± 6 μm), HFCSN1 (158 ± 16 and 77 ± 7 μm), HFCSN2 (155 ± 15 and 80 ± 11 μm), CCSN1 (174 ± 11 and 91 ± 10 μm) and CCSN2 (190 ± 19 and 93 ± 7 μm) than those of unstimulated cells on AFCSN1 (81 ± 9 and 48 ± 7 μm), AFCSN2 (80 ± 7 and 48 ± 4 μm), HFCSN1 (87 ± 7 and 51 ± 5 μm), HFCSN2 (84 ± 6 and 55 ± 8 μm), CCSN1 (97 ± 6 and 61 ± 7 μm) and CCSN2 (101 ± 6 and 64 ± 5 μm) and the differences were statistically significant at $p<0.01$ [**Figure 12 (i) & (j)**]. The neurite length per cell under electrical stimulation was statistically different at $p<0.05$ between AFCSN1 *vs* CCSN1 and HFCSN1 *vs* CCSN1 and at $p<0.01$ between AFCSN2 *vs* CCSN2 and HFCSN2 *vs* CCSN2. Similarly, the median neurite length under electrical stimulation was statistically different at $p<0.01$ between AFCSN1 *vs* CCSN1, AFCSN2 *vs* CCSN2 and HFCSN2 *vs* CCSN2, while the same was significant between HFCSN1 *vs* CCSN1 at $p<0.05$ [**Figure 12 (i) & (j)**]. Thus, the statistical analysis using two-way ANOVA analysis further demonstrated that the collagen coating along with the electrical stimulation played a vital role in axonal growth. However, surface functionalization along with the electrical stimulation contributed towards the significant enhancement in the neurite formation and the axonal growth when compared to those on the collagen coated meshes under no electrical stimulation. The statistical analysis showed that the percentage of neurite bearing cells, the neurite per cell, the neurite length per and the median neurite length were significantly different at $p<0.01$ on the electrically stimulated surface functionalized meshes from those on the collagen coated meshes under no electrical stimulation.

Discussion. It has been reported that the amine functionality makes the surface positively charged, which ultimately encourages the electrostatic interactions with the negatively charged cell surface. Moreover, the amine functionality can interact with the carboxyl terminus of integrin proteins on the cell surface through amide bond formation. Thereby, the incorporation of amine functionality after surface functionalization by APTES and 1,6-hexanediamine improves the bioactivity of the core-sheath MEH-PPV:PCL nanofibres for better cell-biomaterial interactions, which yields enhanced fibroblast adhesion, spreading, and proliferation. However, PC12 cells have been demonstrated to adhere less on these surface functionalized meshes and subsequently, the neural differentiation rate was also lower than on the collagen coated meshes. It implies only amine functionality on the surface is unable to provide proper binding motifs for neural differentiation of the PC12 cells. Surprisingly, surface functionalization along with the electrical stimulation approach demonstrated almost comparable neural differentiation and neurite outgrowth of PC12 cells than that on the collagen coated meshes. Nonetheless, electrical stimulation through the surface functionalized and collagen coated electrically conductive MEH-PPV:PCL meshes yielded enhanced neurite formation and neurite outgrowth when compared to the unstimulated cells.

Generally, aligned fibrous scaffold is highly desirable for neural applications. The aligned morphology of the nanofibres could further enhance their functional performances as smart biomaterial scaffold; particularly towards unidirectional electrically stimulation guided axonal regeneration.[6,12,33,41] Interestingly, the current study on electrically stimulated neural differentiation of PC12 cells and the neurite outgrowth through amine functionalized randomly oriented core MEH-PPV:PCL sheath electrospun nanofibers showed better outcome when compared to the some of the reports dealing with aligned fibrous scaffolds. For example, Jing *et*

al. reported the median neurite length of PC12 cells on aligned PLGA and PPy coated PLGA fibers were 36.67 ± 19.6 μm and 40.25 ± 13.56 μm[99], respectively, after 7 days of culture without stimulation, which were much less than demonstrated in the present study (48-64 μm under no electrical stimulation and 66-93 μm under electrical stimulation). Zhang *et. al.* demonstrated median neurite length of 19.7 μm and percentage of neurite bearing cells upto 40.5 ± 3.9% of PC12 cells cultured on the aligned (P(LLA-CL))/silk fibroin blend with PAni under electrical potential of 100 mV/cm for 1 h/day for 5 continuous days.[39] Liu *et. al.* showed neurite outgrowth upto 100-150 mm on polypyrrole/poly(styrene-β-isobutylene-β-styrene) aligned fiber,[100] whereas the present study demonstrated neurite outgrowth upto 136-190 mm under electrical stimulation. In addition, some of the aligned scaffolds of non-conductive biomaterials adopting similar experimental procedure as in the current study showed less neurite formation and outgrowth.[32,101,102] Lee *et. al.* and Xia *et. al.* also did not observe any significant difference in neurite formation with PC12 cells and dorsal root ganglia cells on aligned and random fibrous scaffold.[41,43] Lee *et. al.*, however, reported slight enhancement in the percentage of neurite bearing cells and median neurite length with PC12 cells under electrical stimulation through aligned PPy/PLGA fibers as compared to those on the random PPy/PLGA fibers. Considering all these observations along with the findings of the current study, it is evident that external electrical stimulation has a dominating role on neurite formation and outgrowth than the fiber orientation.

The exact mechanisms of the electrical signal on neurite formation and outgrowth are still unknown. There have been several hypotheses postulated to describe the effect of electrical signal on cellular functions, particularly on nerve regeneration. Patel *et al.* reported that electrical stimulation causes electrophoretic redistribution of cell membrane growth factor and adhesion

receptors or cytoskeletal proteins such as actin and subsequent accumulation on the working electrode.[103] Kotwal *et al.* also showed enhanced neurite extension on PPy films due to electrically stimulated fibronectin adsorption.[104] Thus, the electrophoretic accumulation or the electrically stimulated serum protein adsorption during *in vitro* experiment may yield enhanced cell-biomaterial adhesion, which is also evident from the observation that under electrical stimulation, there are more cells available for analysis on the surface functionalized electrospun meshes than under no electrical stimulation. Other possible mechanisms of electrically stimulated neurite growth are direct depolarization or hyperpolarization of nerves leading to the activation of growth-controlling transport processes across the plasma membrane,[105] conformational modifications of membrane or extracellular matrix protein,[106] and enhancement of protein synthesis.

The chronoamperometric current signal applied in pulse mode during electrical stimulation through different electrospun meshes were shown in **Figure S12 in SI**. The results reveal a systematic increase in the neurite formation and extension with increase in current signal (up to 8-9 μA) through the conductive electrospun scaffolds during stimulation in the order of CCSN2>CCSN1>HFCSN2>AFCSN2>HFCSN1>AFCSN1 [**Figure S12**]. This order again is according to the surface resistivity (ρ) of the individual meshes as shown in Table I. Moreover, it has been also observed that surface functionalized meshes revealed enhanced PC12 adhesion under electrical stimulation as the number of cells available for analysis under electrical stimulation was greater than those under no electrical stimulation. This observation is supported by the findings of Zhang *et al.* that the current below 10 μA encourages more neurite formation and above 10 μA, the degree of neurite formation is less.[41] The analysis of *I-V* characteristics results demonstrated that CSN2 and its functionalized counterparts had slightly lower *Vc* values

[Table I] and indicated higher density of free charge carriers in them. Therefore, these meshes facilitate more charge-transport between the scaffold and the cell membrane, resulting in slightly more neurite formation and outgrowth when compared to CCSN1 and its functionalized counterparts as shown in **Figure 12**. This charge-transport process changes the resting membrane potential of differentiated PC12 cells. Under constant electrical potential for 2 h, the cell membrane undergoes an intensity-dependent depolarization resulting action potential, which is responsible for axonal growth. Furthermore, such membrane depolarization can also induce Ca^{2+} influx into PC12 cells that activates protein kinase C.[106] It has been shown that membrane depolarization induces neurite outgrowth due to an elevated concentration of K^+.[107] The elevated concentration of K^+ are further believed to induce immediate early genes (IEGs), that are responsible for depolarization of neuronal cells and differentiation.[108] Cavalie *et. al* showed that extracellular Ca^{2+} influx is required to induce IEGs by depolarization.[109] Kimura *et. al* showed that electrically induced *c-fos* mRNA expression due to Ca^{2+} influx via an L-type calcium ion channel causes differentiation of PC12 cells without NGF.[108] It has been demonstrated that the elevated concentration of K^+ induces differentiation of PC12 cells through Ras cascade in which association and phosphorylation of EGF (epidermal growth factor) receptor were observed in a Ca^{2+} ion dependent manner.[106,110] Thus, at a high-concentration of K^+ ions, the Ca^{2+} ions play an important and interesting role in neurite outgrowth, which can be ultimately modulated with the help of external electrical signal.

CONCLUSIONS

In our previous report, we showed that electrically conductive MEH-PPV:PCL electrospun nanofibres with collagen coating for electrical stimulation of PC12 cells.[NRef] In this paper, we showed the amine functionalized core-sheath MEH-PPV:PCL nanofibres fabricated by modified

coaxial electrospinning technique to modulate 3T3 cell activities and electrically stimulated neurite formation and outgrowth. Briefly, the nanofibrous features and core-sheath morphology have been confirmed by SEM and TEM analysis, whereas conductive and mechanical properties have been assessed with the help of room temperature I-V characteristics and tensile test. XPS and FTIR confirm incorporation of amine functionality on the surface of the electrospun nanofibres by surface functionalization using APTES and 1,6-hexanedamine. Surface functionalized electrospun meshes retain its conductive properties indicating that conductive properties are not affected by surface functionalization process. The stability test reveals degradation behavior of the functionalized meshes, particularly AFCSN1 and AFCSN2, while the core-sheath nanofibres retain conductive properties after 45 days in physiological solution. Probable interaction mechanisms of surface functionalization have been proposed based on the XPS and FTIR results. Core-sheath nanofibres have been found to be biocompatible as indicated by MTS proliferation assay with 3T3 fibroblasts and PC12 cells. Surface functionalization significantly mediated various cellular activities of 3T3 cells such cell viability, adhesion, spreading and migration as demonstrated by quantitative analysis of live/dead assay and cell adhesion test. PC12 neuronal-like cells differentiated well and demonstrated significant improvement in neurite formation and outgrowth on collagen-coated samples than that on the uncoated samples. However, surface functionalized nanofibres favor better differentiation of PC12 cells than the non-functionalized meshes, but less than the collagen-coated samples. Electrical stimulation of PC12 cells through the electrically conductive meshes under the potential of 500 mV/cm for 2 h for 3 consecutive days demonstrates significant improvement in neurite formation and outgrowth than the unstimulated PC12 cells. However, the effect of electrical stimulation on PC12 cells cultured on the collagen coated meshes has been found to be

more prominent than that on the surface functionalized meshes. The present study reveals that the surface amination of the core-sheath nanofibres along with electrical stimulation comes out as a promising scaffold to replace the need of coating the scaffold with costly biomolecules such as collagen, laminin, fibronectin etc. The results indicate the potential of MEH-PPV based biomaterial scaffolds in fabrication of nerve guidance channels to bridge the gap for directive growth of damaged nerves in peripheral nervous system (PNS) as an alternative to conventional nerve grafts such as autograft and allograft. In addition to its utility for nerve regeneration, the polymer has potential in other areas of tissue engineering as well, such as skin and connective tissue, wound healing, bone repair, cartilage, and muscle tissue engineering etc. Additionally, MEH-PPV has been assessed for the first time with living cells in direct contact indicating its potential in biomedical applications as alternatives to widely investigated PPy, PANi, and PEDOT, where poor solubility and biodegradability limit their biomedical applications. However, there are scopes in further research in optimizing the surface parameters for the efficient outcome such as in neural tissue engineering.

ACKNOWLEDGEMENTS

The authors cordially acknowledged British Council, UK and Department of Biotechnology, Govt. of India and for the financial support through Newton-Bhabha Scheme to carry out this work at University of Brighton, UK. This research work was also partially supported by Department of Science & Technology (DST), Govt. of India through Inspire Fellowship Scheme. The authors are thankful to Dr. Santanu Ray, School of Environment and Technology, University of Brighton, UK for his help during XPS measurement. The authors also gratefully acknowledge the help extended Dr. Andrew Flint, Image and Analysis unit, University of Brighton during SEM and confocal microscopy.

ASSOCIATED CONTENT

Supporting Information

Supplementary Tables of X-ray diffraction analysis showing domain length and strain, *Kaiser* fitting data; Supplementary Figures show: Schematic illustration and digital photograph of coaxial electrospinning process, Diameter distributions of the core-sheath nanofibers from SEM images, Schematic illustration of electrical stimulation experiment, X-ray diffraction pattern and labeled along with a Voigtian fit of the X-ray profiles, Stress *vs* Strain curve and comparison of Young Modulus or stiffness constant (*E*) and ultimate tensile strength (UTS), Forward *I-V* data on a log-log scale showing fitting parameters according to power law equation, Forward non-linear *I-V* characteristics fitted with *Kaiser Equation*, FT-IR spectra of pure PCL and MEH-PPV, Elemental composition in different MEH-PPV:PCL electrospun nanofibres before and after functionalization along with peak deconvolution of high-resolution C1s XPS spectra of CSN2, AFCSN2 and HFCSN2, Probable interaction mechanisms of MEH-PPV with APTES and MEH-PPV with 1,6-hexanediamine (Scheme II) based on XPS and FT-IR results, Quantitative analysis of 3T3 cell density per field of view on the non-functionalized and functionalized electrospun core-sheath MEH-PPV:PCL meshes, and Current signal recorded (upto 400 s) during electrical stimulation of PC12 cells through the different core-sheath MEH-PPV:PCL electrospun meshes.

REFERENCES

(1) Haastert-Talini, K.; Grothe, C. Electrical stimulation for promoting peripheral nerve regeneration. In International review of neurobiology. *Int. Rev. Neurobiol.* **2013,** *109*, 111-124. DOI: 10.1016/B978-0-12-420045-6.00005-5.

(2) Schmidt, C.E.; Shastri, V.R.; Vacanti, J.P.; Langer, R. Stimulation of neurite outgrowth using an electrically conducting polymer. *Proc. Natl. Acad. Sci.* **1997,** *94(17),* 8948-8953. DOI: 10.1073/pnas.94.17.8948.

(3) Valentini, R.F.; Sabatini, A.M.; Dario, P.; Aebischer, P. Polymer electret guidance channels enhance peripheral nerve regeneration in mice. *Brain Res.* **1989,** *480(1-2),* 300-304. DOI: 10.1016/0006-8993(89)90196-0.

(4) Aebischer, P.; Valentini, R.F.; Dario, P.; Domenici, C.; Galletti, P.M. Piezoelectric guidance channels enhance regeneration in the mouse sciatic nerve after axotomy. *Brain Res.* **1987,** *436(1),* 165-168. DOI: 10.1016/0006-8993(87)91570-8.

(5) Valentini, R.F.; Vargo, T.G.; Gardella Jr, J.A.; Aebischer, P.; Electrically charged polymeric substrates enhance nerve fibre outgrowth *in vitro*. *Biomaterials,* **1992,** *13(3),* 183-190. DOI: 10.1016/0142-9612(92)90069-Z.

(6) Zou, Y.; Qin, J.; Huang, Z.; Yin, G.; Pu, X.; He, D. Fabrication of aligned conducting PPy-PLLA fiber films and their electrically controlled guidance and orientation for neurites. *ACS Appl. Mater. Interfaces,* **2016,** *8(20),* 12576-12582. DOI: 10.1021/acsami.6b00957.

(7) Hardy, J.G.; Cornelison, R.C.; Sukhavasi, R.C.; Saballos, R.J.; Vu, P.; Kaplan, D.L.; Schmidt C.E. Electroactive tissue scaffolds with aligned pores as instructive platforms for biomimetic tissue engineering. *Bioengineering*, **2015,** *2*, 15-34. DOI: 10.3390/bioengineering2010015.

(8) Hardy, J.G.; Villancio-Wolter, M.K.; Sukhavasi, R.C.; Mouser, D.J.; Aguilar, D.; Geissler, S.A.; Kaplan, D.L.; Schmidt C.E. Electrical stimulation of human mesenchymal stem cells on conductive nanofibres enhances their differentiation towards osteogenic

outcomes. *Macromol. Rapid Commun.* **2015,** *36,* 1884-1890. DOI: 10.1002/marc.201500233

(9) Samba, R.; Herrmann, T.; Zeck, G. PEDOT-CNT coated electrodes stimulate retinal neurons at low voltage amplitudes and low charge densities. *J. Neural Eng.* **2015,** *12(1),* 016014. DOI: 10.1088/1741-2560/12/1/016014.

(10) Wang, K.; Fishman, H.A.; Dai, H.; Harris, J.S. Neural stimulation with a carbon nanotube microelectrode array. *Nano Lett.* **2006,** *6(9),* 2043-2048. DOI: 10.1021/nl061241t.

(11) Li, N.; Zhang, Q.; Gao, S.; Song, Q.; Huang, R.; Wang, L.; Liu, L.; Dai, J.; Tang, M.; Cheng, G. Three-dimensional graphene foam as a biocompatible and conductive scaffold for neural stem cells. *Sci. Rep.* **2013,** *3,* 1604. DOI: 10.1038/srep01604.

(12) Yan, L.; Zhao, B.; Liu, X.; Li, X.; Zeng, C.; Shi, H.; Xu, X.; Lin, T.; Dai, L.; Liu, Y. Aligned nanofibers from polypyrrole/graphene as electrodes for regeneration of optic nerve via electrical stimulation. *ACS Appl. Mater. Interfaces,* **2016,** *8(11),* 6834-6840. DOI: 10.1021/acsami.5b12843.

(13) Wong, J.Y.; Langer, R.; Ingber, D.E. Electrically conducting polymers can noninvasively control the shape and growth of mammalian cells. *Proc. Natl. Acad. Sci.* **1994,** *91(8),* 3201-3204. DOI: 10.1073/pnas.91.8.3201.

(14) Ravichandran, R.; Sundarrajan, S.; Venugopal, J.R.; Mukherjee, S.; Ramakrishna, S. Applications of conducting polymers and their issues in biomedical engineering. *J. R. Soc. Interface,* **2010,** p.rsif20100120. DOI: 10.1098/rsif.2010.0120.focus.

(15) Gopinathan, J.; Quigley, A.F.; Bhattacharyya, A.; Padhye, R.; Kapsa, R.M.; Nayak, R.; Shanks, R.A.; Houshyar, S. Preparation, characterisation, and *in vitro* evaluation of

electrically conducting poly (ε-caprolactone)-based nanocomposite scaffolds using PC12 cells. *J. Biomed. Mater. Res. Part A,* **2016,** *104(4),* 853-865. DOI: 10.1002/jbm.a.35620.

(16) Zhao, Q.; Xin, Y.; Huang, Z.; Liu, S.; Yang, C.; Li, Y. Using poly [2-methoxy-5-(2′-ethyl-hexyloxy)-1,4-phenylene vinylene] as shell to fabricate the highly fluorescent nanofibers by coaxial electrospinning. *Polymer,* **2007,** *48(15),* 4311-4315. DOI: 10.1016/j.polymer.2007.04.068.

(17) Matharu, Z.; Arya, S. K.; Singh, S. P.; Gupta, V.; Malhotra, B. D. Langmuir–Blodgett film based on MEH-PPV for cholesterol biosensor. *Anal. Chim. Acta,* **2009,** *634(2),* 243-249. DOI: 10.1016/j.aca.2008.12.023.

(18) Borah, R.; Ingavle, G.; Sandeman, S. R.; Kumar, A.; Mikhalovsky, S. Electrically Conductive MEH-PPV: PCL Electrospun Nanofibers for Electrical Stimulation of Rat PC12 Pheochromocytoma Cells. *Biomater. Sci.* **2018,** DOI: 10.1039/C8BM00559A. DOI: 10.1039/C8BM00559A.

(19) Prabhakaran, M. P.; Ghasemi-Mobarakeh, L.; Ramakrishna, S. Electrospun composite nanofibers for tissue regeneration. *J. Nanosci. Nanotechnol.* **2011,** *11(4),* 3039-3057. DOI: 10.1166/jnn.2011.3753.

(20) Wang, Q.; Yu, D.G.; Zhang, L.L.; Liu, X.K.; Deng, Y.C.; Zhao, M. Electrospun hypromellose-based hydrophilic composites for rapid dissolution of poorly water-soluble drug. *Carbohydr. Polym.* **2017,** *174,* 617-625. DOI: 10.1016/j.carbpol.2017.06.075.

(21) Xu, Y.; Li, J.J.; Yu, D.G.; Williams, G.R.; Yang, J.H.; Wang, X. Influence of the drug distribution in electrospun gliadin fibres on drug-release behavior. *Eur. J. Pharm. Sci.* **2017,** *106,* 422-430. DOI: 10.1016/j.ejps.2017.06.017.

(22) Jin, M.; Yu, D.G.; Wang, X.; Geraldes, C.F.; Williams, G.R.; Bligh, S.A. Electrospun Contrast-Agent-Loaded Fibres for Colon-Targeted MRI. *Adv. Healthcare Mater.* **2016,** *5(8),* 977-985. DOI: 10.1002/adhm.201500872.

(23) Zhao, Y.; Zhang, Z.; Yu, L.; Tang, Q. Electrospinning of polyaniline microfibers for anticorrosion coatings: An avenue of enhancing anticorrosion behaviors. *Synth. Met.* **2016,** *212,* 84-90. DOI: 10.1016/j.synthmet.2015.12.007.

(24) Merlini, C.; Pegoretti, A.; Araujo, T.M.; Ramoa, S.D.; Schreiner, W.H.; de Oliveira Barra, G.M. Electrospinning of doped and undoped-polyaniline/poly (vinylidene fluoride) blends. *Synth. Met.* **2016,** 213, 34-41. DOI: 10.1016/j.synthmet.2015.12.024.

(25) de Castro, J.G.; Rodrigues, B.V.; Ricci, R.; Costa, M.M.; Ribeiro, A.F.; Marciano, F.R.; Lobo, A.O. Designing a novel nanocomposite for bone tissue engineering using electrospun conductive PBAT/polypyrrole as a scaffold to direct nanohydroxyapatite electrodeposition. *RSC Adv.* **2016,** *6(39),* 32615-32623. DOI: 10.1039/C6RA00889E.

(26) Zhou, J.; Cheng, L.; Sun, X.; Wang, X.; Jin, S.; Li, J.; Wu, Q. Neurogenic differentiation of human umbilical cord mesenchymal stem cells on aligned electrospun polypyrrole/polylactide composite nanofibers with electrical stimulation. *Frontiers of Materials Science*, **2016,** *10(3),* 260-269. DOI: 10.1007/s11706-016-0348-6.

(27) Bessaire, B.; Mathieu, M.; Salles, V.; Yeghoyan, T.; Celle, C.; Simonato, J.P.; Brioude, A. Synthesis of continuous conductive PEDOT:PSS nanofibers by electrospinning: a conformal coating for optoelectronics. *ACS Appl. Mater. Interfaces,* **2016,** *9(1),* 950-957. DOI: 10.1021/acsami.6b13453.

(28) Liu, X.; Shao, W.; Luo, M.; Bian, J.; Yu, D.G. Electrospun blank nanocoating for improved sustained release profiles from medicated gliadin nanofibres. *Nanomaterials,* **2018,** *8(4),* 184. DOI: 10.3390/nano8040184.

(29) Yang, Y.Y.; Liu, Z.P.; Yu, D.G.; Wang, K.; Liu, P.; Chen, X. Colon-specific pulsatile drug release provided by electrospun shellac nanocoating on hydrophilic amorphous composites. *Int. J. Nanomed.* **2018,** *13,* 2395. DOI: 10.2147/IJN.S154849.

(30) Jin, M.; Yu, D.G.; Geraldes, C.F.; Williams, G.R.; Bligh, S.A. Theranostic fibres for simultaneous imaging and drug delivery. *Mol. Pharmaceutics,* **2016,** *13(7),* 2457-2465. DOI: 10.1021/acs.molpharmaceut.6b00197.

(31) Tian, L.; Prabhakaran, M.P.; Hu, J.; Chen, M.; Besenbacher, F.; Ramakrishna, S. Coaxial electrospun poly(lactic acid)/silk fibroin nanofibres incorporated with nerve growth factor support the differentiation of neuronal stem cells. *RSC Adv.* **2015,** *5(62),* 49838-49848. DOI: 10.1039/C5RA05773F.

(32) Hu, J.; Tian, L.; Prabhakaran, M.P.; Ding, X.; Ramakrishna, S. Fabrication of nerve growth factor encapsulated aligned poly (ε-caprolactone) nanofibres and their assessment as a potential neural tissue engineering scaffold. *Polymers,* **2016,** *8(2),* 54. DOI: 10.3390/polym8020054.

(33) Wang, C.Y.; Liu, J.J.; Fan, C.Y.; Mo, X.M.; Ruan, H.J.; Li, F.F. The effect of aligned core–shell nanofibres delivering NGF on the promotion of sciatic nerve regeneration. *J. Biomater. Sci., Polym. Ed.* **2012,** *23(1-4),* 167-184. DOI: 10.1163/092050610X545805.

(34) Taghipoor, F.; Semnani, D.; Naghashzargar, E.; Rezaei, B. Electrochemical properties of bi-component bundle of coaxial polyacrylonitrile/polyaniline nanofibres containing TiO_2

nanoparticles. *J. Compos. Mater.* **2017,** *51(24),* 3355-3363. DOI: 10.1177/0021998316687028.

(35) Xi, X.; Ma, Q.; Dong, X.; Li, D.; Yu, W.; Wang, J.; Liu, G. Electrospinning assembly of 1D peculiar Janus nanofibre into 2D anisotropic electrically conductive array membrane synchronously endued with tuned superparamagnetism and color-tunable luminescence. *J. Mater. Sci.: Mater. Electron.* **2018,** *29(12),* 10284-10300. DOI: 10.1007/s1085.

(36) Liu, P.; Wu, S.; Zhang, Y.; Zhang, H.; Qin, X. A fast response ammonia sensor based on coaxial PPy–PAN nanofibre yarn. *Nanomaterials,* **2016,** *6(7),* 121. DOI: 10.3390/nano6070121.

(37) Moreno-Cortez, I.E.; Alvarado-Castaneda, A.; Garcia-Gutierrez, D.F.; Garcia-Gomez, N.A.; Sepulveda-Guzman, S.; Garcia-Gutierrez, D.I. Core–shell PEDOT: PSS-PVP nanofibres containing PbS nanoparticles through coaxial electrospinning. *Synth. Met.* **2016,** *220,* 255-262. DOI: 10.1016/j.synthmet.2016.06.019.

(38) Lin, M.F.; Don, T.M.; Chang, F.T.; Huang, S.R.; Chiu, W.Y. Preparation and properties of thermoresponsive and conductive composite fibres with core-sheath structure. *J. Polym. Sci., Part A: Polym. Chem.* **2016,** *54(9),* 1299-1307. DOI: 10.1002/pola.27976.

(39) Zhang, J.; Qiu, K.; Sun, B.; Fang, J.; Zhang, K.; Hany, E.H.; Al-Deyab, S.S.; Mo, X. The aligned core–sheath nanofibres with electrical conductivity for neural tissue engineering. *J. Mater. Chem. B,* **2014,** *2(45),* 7945-7954. DOI: 10.1039/C4TB01185F.

(40) Lee, J.Y.; Bashur, C.A.; Milroy, C.A.; Forciniti, L.; Goldstein, A.S.; Schmidt C.E. Nerve growth factor-immobilized electrically conducting fibrous scaffolds for potential use in neural engineering applications. *IEEE Transactions on NanoBioscience*, **2012,** *11(1)*, 15-21. DOI: 10.1109/TNB.2011.2159621.

(41) Lee, J.Y.; Bashur, C.; Goldstein, A.; Schmidt, C.E. Polypyrrole-coated electrospun PLGA nanofibres for neural tissue applications. *Biomaterials,* **2009,** *30(26)*, 4325-35. DOI: 10.1016/j.biomaterials.2009.04.042.

(42) Chen, C.; Chen, X.; Zhang, H.; Zhang, Q.; Wang, L.; Li, C.; Dai, B.; Yang, J.; Liu, J.; Sun, D. Electrically-responsive core-shell hybrid microfibers for controlled drug release and cell culture. *Acta Biomater.* **2017,** *55,* 434-442. DOI: 10.1016/j.actbio.2017.04.005.

(43) Xie, J.; MacEwan, M.R.; Willerth, S.M.; Li, X.; Moran, D.W.; Sakiyama-Elbert, S.E.; Xia, Y. Conductive core–sheath nanofibers and their potential application in neural tissue engineering. *Adv. Funct. Mater.* **2009,** *19(14),* 2312-2318. DOI: 10.1002/adfm.200801904.

(44) Zhou, X.; Yang, A.; Huang, Z.; Yin, G.; Pu, X.; Jin, J. Enhancement of neurite adhesion, alignment and elongation on conductive polypyrrole-poly(lactide acid) fibers with cell-derived extracellular matrix. *Colloids Surf., B,* **2017,** *149,* 217-225. DOI: 10.1016/j.colsurfb.2016.10.014.

(45) Mondal, D.; Griffith, M.; Venkatraman, S.S. Polycaprolactone-based biomaterials for tissue engineering and drug delivery: Current scenario and challenges. *Int. J. Polym. Mater. Polym. Biomater.* **2016,** *65(5),* 255-265. DOI: 10.1080/00914037.2015.1103241.

(46) Gao, X.; Song, J.; Ji, P.; Zhang, X.; Li, X.; Xu, X.; Wang, M.; Zhang, S.; Deng, Y.; Deng, F.; Wei, S. Polydopamine-templated hydroxyapatite reinforced polycaprolactone composite nanofibers with enhanced cytocompatibility and osteogenesis for bone tissue engineering. *ACS Appl. Mater. Interfaces,* **2016,** *8(5),* 3499-3515. DOI: 10.1021/acsami.5b12413.

(47) Yang, G.; Lin, H.; Rothrauff, B.B.; Yu, S.; Tuan, R.S. Multilayered polycaprolactone/gelatin fiber-hydrogel composite for tendon tissue engineering. *Acta Biomater.* **2016,** *35,* 68-76. DOI: 10.1016/j.actbio.2016.03.004.

(48) Spearman, B.; Hodge, A.J.; Porter, J.; Hardy, J.G.; Davis, Z.; Xu, T.; Zhang, X.; Schmidt, C.E.; Hamilton, M.C.; Lipke E.A. Conductive interpenetrating networks of polypyrrole and polycaprolactone encourage electrophysiological development of cardiac cells. *Acta Biomater.* **2015, 28,** 109-120. DOI: 10.1016/j.actbio.2015.09.025.

(49) Santos, E.; Orive, G.; Hernández, R. M.; Pedraz, J. L. Cell-biomaterial interaction: strategies to mimic the extracellular matrix; Pramatarova, L. (Eds.); InTech.: Bulgaria, **2011,** 529-558. DOI: 10.5772/21634.

(50) García, A. J. Get a grip: integrins in cell-biomaterial interactions. *Biomaterials,* **2005,** *26,* 7525-7529. DOI: 10.1016/j.biomaterials.2005.05.029.

(51) Nickels, J.D.; Schmidt, C.E. Surface modification of the conducting polymer, polypyrrole, via affinity peptide. *J. Biomed. Mater. Res.* **2013,** *101(5),* 1464-1471. DOI: 10.1002/jbm.a.34435.

(52) Chua, P.H.; Neoh, K.G.; Kang, E.T.; Wang, W. Surface functionalization of titanium with hyaluronic acid/chitosan polyelectrolyte multilayers and RGD for promoting osteoblast functions and inhibiting bacterial adhesion. *Biomaterials,* **2008,** *29(10),* 1412-1421. DOI: 10.1016/j.biomaterials.2007.12.019.

(53) Lee, J. H.; Lee, J. W.; Khang, G.; Lee, H. B. Interaction of cells on chargeable functional group gradient surfaces. *Biomaterials,* **1997,** *18(4),* 351-358. DOI: 10.1016/S0142-9612(96)00128-7.

(54) Lee, J.Y.; Schmidt, C.E. Amine-functionalized polypyrrole:inherently cell adhesive conducting polymer. *J. Biomed. Mater. Res., Part A,* **2015,** *103(6),* 2126-32. DOI: 10.1002/jbm.a.35344.

(55) Arnold, K.; Davies, B.; Giles, R. L.; Grosjean, C.; Smith, G. E.; Whiting, A. To catalyze or not to catalyze? Insight into direct amide bond formation from amines and carboxylic acids under thermal and catalyzed conditions. *Adv. Synth. Catal.* **2006,** *348(7-8)*, 813-820. DOI: 10.1002/adsc.200606018.

(56) Mansur, H. S.; Oréfice, R. L.; Vasconcelos, W. L.; Lobato, Z. P.; Machado, L. J. C. Biomaterial with chemically engineered surface for protein immobilization. *J. Mater. Sci.: Mater. Med.* **2005,** *16(4),* 333-340. DOI: 10.1007/s10856-005-0632-y.

(57) Reyes, C.D.; García, A.J. Engineering integrin-specific surfaces with a triple-helical collagen-mimetic peptide. *J. Biomed. Mater. Res., Part A,* **2003,** *65(4),* 511-523. DOI: 10.1002/jbm.a.10550.

(58) Mulder, L.; Baaijens, F.P.T.; Bouten, C.V.C.; van Lieshout (MI). Cell adhesion on alginate scaffolds for the tissue engineering of an aortic valve: a review. Technische Universiteit Eindhoven, **2002**.

(59) Zhu, M.; Lerum, M. Z.; Chen, W. How to prepare reproducible, homogeneous, and hydrolytically stable aminosilane-derived layers on silica. *Langmuir,* **2011,** *28(1),* 416-423. DOI: 10.1021/la203638g.

(60) Geszke-Moritz, M.; Moritz, M. APTES-modified mesoporous silicas as the carriers for poorly water-soluble drug. Modeling of diflunisal adsorption and release. *Appl. Surf. Sci.* **2016,** *368,* 348-359. DOI: 10.1016/j.apsusc.2016.02.004.

(61) Fan, D.; De Rosa, E.; Murphy, M. B.; Peng, Y.; Smid, C. A.; Chiappini, C.; Liu, X.; Simmons, P.; Weiner, B. K.; Ferrari, M.; Tasciotti, E. Mesoporous silicon-PLGA composite microspheres for the double controlled release of biomolecules for orthopedic tissue engineering. *Adv. Funct. Mater.* **2012,** *22(2),* 282-293. DOI: 10.1002/adfm.201100403.

(62) Ding, C.; Liu, Y.; Wang, T.; Fu, J. Triple-stimuli-responsive nanocontainers assembled by water-soluble pillar [5] arene-based pseudorotaxanes for controlled release. *J. Mater. Chem. B,* **2016,** *4(16),* 2819-2827. DOI: 10.1039/C6TB00459H.

(63) Sakiyama, S.; Mizutani, N.; Fujita, K. Controllable p-and n-type doping of poly [2-methoxy-5-(2′-methyl-hexyloxy)-p-phenylenevinylene] films prepared by evaporative spray deposition using ultra-dilute solution. *Jpn. J. Appl. Phys.* **2016,** *55(4S),* 04EL03. DOI: 10.7567/JJAP.55.04EL03.

(64) Li, W. A.; Lu, B. Y.; Gu, L.; Choi, Y.; Kim, J.; Mooney, D. J. The effect of surface modification of mesoporous silica micro-rod scaffold on immune cell activation and infiltration. *Biomaterials,* **2016,** *83,* 249-256. DOI: 10.1016/j.biomaterials.2016.01.026.

(65) Santiago, L. Y.; Nowak, R. W.; Rubin, J. P.; Marra, K. G. Peptide-surface modification of poly (caprolactone) with laminin-derived sequences for adipose-derived stem cell applications. *Biomaterials,* **2006,** *27(15),* 2962-2969. DOI: 10.1016/j.biomaterials.2006.01.011.

(66) Barltrop, J. A.; Owen, T. C.; Cory, A. H.; Cory, J. G. 5-(3-carboxymethoxyphenyl)-2-(4, 5-dimethylthiazolyl)-3-(4-sulfophenyl) tetrazolium, inner salt (MTS) and related analogs of 3-(4,5-dimethylthiazolyl)-2,5-diphenyltetrazolium bromide (MTT) reducing to purple

water-soluble formazans as cell-viability indicators. *Bioorg. Med. Chem. Lett.* **1991,** *11,* 611-614. DOI: 10.1016/S0960-894X(01)81162-8.

(67) Cheng, H.; Yue, K.; Kazemzadeh-Narbat, M.; Liu, Y.; Khalilpour, A.; Li, B.; Zhang, Y.S.; Annabi, N.; Khademhosseini, A. Mussel-inspired multifunctional hydrogel coating for prevention of infections and enhanced osteogenesis. *ACS Appl. Mater. Interfaces,* **2017,** *9(13),* 11428-11439. DOI: 10.1021/acsami.6b16779.

(68) Huishang, Y.; Zhu, G.; Huang, Y.; Shi, X.; Wang, Y. The stimulation of the differentiation of pheochromocytoma (PC12-L) cells into neuron-like cells by electrically conductive nanofibre mesh. *Applied Materials Today,* **2016,** *5*, 215-222. DOI: 10.1016/j.apmt.2016.09.017.

(69) Bashur, C. A.; Dahlgren, L. A.; Goldstein, A. S. Effect of fiber diameter and orientation on fibroblast morphology and proliferation on electrospun poly (D, L-lactic-co-glycolic acid) meshes. *Biomaterials*, **2006,** *27(33),* 5681-5688. DOI: 10.1016/j.biomaterials.2006.07.005.

(70) Min, B. M.; Lee, G.; Kim, S. H.; Nam, Y. S.; Lee, T. S.; Park, W. H. Electrospinning of silk fibroin nanofibers and its effect on the adhesion and spreading of normal human keratinocytes and fibroblasts *in vitro*. *Biomaterials*, **2004,** *25(7),* 1289-1297. DOI: 10.1016/j.biomaterials.2003.08.045.

(71) Gladwin, K.M.; Whitby, R.L., Mikhalovsky, S.V.; Tomlins, P.; Adu, J. *In vitro* biocompatibility of multiwalled carbon nanotubes with sensory neurons. *Adv. Healthcare Mater.* **2013,** *2(5),* 728-735. DOI: 10.1002/adhm.201200233.

(72) Cen, L.; Neoh, K.G.; Kang, E.T. Surface functionalization of electrically conductive polypyrrole film with hyaluronic acid. *Langmuir,* **2002,** *18(22),* 8633-8640. DOI: 10.1021/la025979b.

(73) Pham, Q.P.; Sharma, U.; Mikos, A. G. Electrospinning of polymeric nanofibers for tissue engineering applications: a review. *Tissue Eng.* **2006,** *12(5),* 1197-1211. DOI: 10.1089/ten.2006.12.1197.

(74) Hazarika, J. and Kumar, A. Scalable and low cost synthesis of highly conducting polypyrrole nanofibers using oil–water interfacial polymerization under constant stirring. *J. Phys. Chem. B,* **2017,** *121(28),* 6926-6933. DOI: 10.1021/acs.jpcb.7b03179.

(75) Lampert, M. A. and Mark, P. *Current Injection in Solids*, Academic, New York, USA, **1970**.

(76) Kao, K. C. and Hwang, W. *Electrical Transport in Solids.* Pergamon Press, New York, USA, **1981**.

(77) Choi, K.H.; Kim, H.B.; Ali, K.; Sajid, M.; Siddiqui, G.U.; Chang, D.E.; Kim, H.C.; Ko, J.B.; Dang, H.W.; Doh, Y.H. Hybrid surface acoustic wave-electro hydrodynamic atomization (SAW-EHDA) for the development of functional thin films. *Sci. Rep.* **2015,** *5*. DOI: 10.1038/srep15178.

(78) Roque, A. P.; Mercante, L. A.; Scagion, V. P.; Oliveira, J. E.; Mattoso, L. H.; Boni, L.; Mendonca, C. R.; Correa, D. S. Fluorescent PMMA/MEH-PPV electrospun nanofibers: Investigation of morphology, solvent, and surfactant effect. *J. Polym. Sci., Part B: Polym. Phys.* **2014,** *52(21),* 1388-1394. DOI: 10.1002/polb.23574.

(79) Juhari, N.; Majid, W.H.A.; Ibrahim, Z.A. Structural and optical studies of MEH-PPV using two different solvents prepared by spin coating technique. *Solid State Sci. Technol.* **2007,** *15(1),* 141-146.

(80) Elzein, T.; Nasser-Eddine, M.; Delaite, C.; Bistac, S.; Dumas, P. FTIR study of polycaprolactone chain organization at interfaces. *J. Colloid Interface Sci.* **2004,** *273(2),* 381-387. DOI: 10.1016/j.jcis.2004.02.001.

(81) Benkaddour, A.; Jradi, K.; Robert, S.; Daneault, C. Grafting of polycaprolactone on oxidized nanocelluloses by click chemistry. *Nanomaterials,* **2013,** *3(1),* 141-157. DOI: 10.3390/nano3010141.

(82) Tang, Z. G.; Black, R. A.; Curran, J. M.; Hunt, J. A.; Rhodes, N. P.; Williams, D. F. Surface properties and biocompatibility of solvent-cast poly[ε-caprolactone] films. *Biomaterials,* **2004,** *25(19),* 4741-4748. DOI: 10.1016/j.biomaterials.2003.12.003.

(83) Majoul, N.; Aouida, S.; Bessaïs, B. Progress of porous silicon APTES-functionalization by FTIR investigations. *Appl. Surf. Sci.* **2015,** *331,* 388-391. DOI: 10.1016/j.apsusc.2015.01.107.

(84) López-Pérez, P. M.; Marques, A. P.; da Silva, R. M.; Pashkuleva, I.; Reis, R. L. Effect of chitosan membrane surface modification via plasma induced polymerization on the adhesion of osteoblast-like cells. *J. Mater. Chem.* **2007,** *17(38),* 4064-4071. DOI: 10.1039/B707326G.

(85) Ray, S.; Shard, A. G. Quantitative analysis of adsorbed proteins by X-ray photoelectron spectroscopy. *Anal. Chem.* **2011,** *83(22),* 8659-8666. DOI: 10.1021/ac202110x.

(86) Louette, P.; Bodino, F.; Pireaux, J. J. Poly (caprolactone) (PCL) XPS reference core level and energy loss spectra. *Surf. Sci. Spectra,* **2005,** *12(1),* 27-31. DOI: 10.1116/11.20050906.

(87) Yuan, S.; Xiong, G.; Roguin, A.; Teoh, S.H.; Choong, C. Amelioration of blood compatibility and endothelialization of polycaprolactone substrates by surface-initiated atom transfer radical polymerization. *Advances in biomaterials science and biomedical application*s, InTech, **2013**. DOI: 10.5772/52646.

(88) Pires, F.; Ferreira, Q.; Rodrigues, C. A. V.; Morgado, J.; Ferreira, F. C. Neural stem cell differentiation by electrical stimulation using a cross-linked PEDOT substrate: expanding the use of biocompatible conjugated conductive polymers for neural tissue engineering. *Biochim. Biophys. Acta, Gen. Subj.* **2015,** *1850,* 1158-1168. DOI: 10.1016/j.bbagen.2015.01.020.

(89) Bae, S.H., Che, J.H., Seo, J.M., Jeong, J., Kim, E.T., Lee, S.W., Koo, K.I., Suaning, G.J., Lovell, N.H., Kim, S.J. and Chung, H. *In vitro* biocompatibility of various polymer-based microelectrode arrays for retinal prosthesis. *Invest. Ophthalmol. Visual Sci.*, **2012,** *53*(6), 2653-2657. DOI: 10.1167/iovs.11-9341.

(90) Yoo, H.S.; Kim, T.G.; Park, T.G.; Surface-functionalized electrospun nanofibers for tissue engineering and drug delivery. *Adv. Drug Delivery Rev.* **2009,** *61(12),* 1033-1042. DOI: 10.1016/j.addr.2009.07.007.

(91) Wender, P.A.; Mitchell, D.J.; Pattabiraman, K.; Pelkey, E.T.; Steinman, L.; Rothbard, J.B. The design, synthesis, and evaluation of molecules that enable or enhance cellular uptake: peptoid molecular transporters. *Proc. Natl. Acad. Sci.* **2000,** *97(24),* 13003-13008. DOI: 10.1073/pnas.97.24.13003.

(92) Chen, M.; Patra, P. K.; Warner, S. B.; Bhowmick, S. Role of fiber diameter in adhesion and proliferation of NIH 3T3 fibroblast on electrospun polycaprolactone scaffolds. *Tissue Eng.* **2007,** *13(3),* 579-587. DOI: 10.1089/ten.2006.0205.

(93) Badami, A. S.; Kreke, M. R.; Thompson, M. S.; Riffle, J. S.; Goldstein, A.S. Effect of fiber diameter on spreading, proliferation, and differentiation of osteoblastic cells on electrospun poly (lactic acid) substrates. *Biomaterials,* **2006,** *27(4),* 596-606. DOI: 10.1016/j.biomaterials.2005.05.084.

(94) McFadden, P.N.; Koshland, D.E. Habituation in the single cell: Diminished secretion of norepinephrine with repetitive depolarization of PC12 cells. *Proc. Natl. Acad. Sci.* **1990,** *87(5),* 2031-2035.

(95) Koopmans, G.; Hasse, B.; Sinis, N. The role of collagen in peripheral nerve repair. *Int. Rev. Neurobiol.* **2009,** *87,* 363-379. DOI: 10.1016/S0074-7742(09)87019-0.

(96) Rajnicek, A. M.; Robinson, K. R.; McCaig, C. D. The direction of neurite growth in a weak DC electric field depends on the substratum: contributions of adhesivity and net surface charge. *Dev. Biol.* **1998,** *203(2),* 412-423. DOI: 10.1006/dbio.1998.9039.

(97) Fozdar, D. Y.; Lee, J. Y.; Schmidt, C. E.; Chen, S. Selective axonal growth of embryonic hippocampal neurons according to topographic features of various sizes and shapes. *Int. J. Nanomed.* **2011,** *6,* 45. DOI: 10.2147/IJN.S12376.

(98) Mihic, A.; Cui, Z.; Wu, J.; Vlacic, G.; Miyagi, Y.; Li, S.H.; Lu, S.; Sung, H.W.; Weisel, R.D.; Li, R.K. A conductive polymer hydrogel supports cell electrical signaling and improves cardiac function after implantation into myocardial infarct. *Circulation,* **2015,** *132(8),* 772-784. DOI: 10.1161/CIRCULATIONAHA.114.014937.

(99) Jing, W.; Ao, Q.; Wang, L.; Huang, Z.; Cai, Q.; Chen, G.; Yang, X.; Zhong, W. Constructing conductive conduit with conductive fibrous infilling for peripheral nerve regeneration. *Chem. Eng. J.* **2018**, *345,* 566-577. DOI: 10.1016/j.cej.2018.04.044.

(100) Liu, X.; Chen, J.; Gilmore, K.J.; Higgins, M.J.; Liu, Y.; Wallace, G.G. Guidance of neurite outgrowth on aligned electrospun polypyrrole/poly (styrene-β-isobutylene-β-styrene) fiber platforms. *J. Biomed. Mater. Res., Part A*, **2010,** *94(4),* 1004-1011. DOI: 10.1002/jbm.a.32675.

(101) Wang, Z.H.; Chang, Y.Y.; Wu, J.G.; Lin, C.Y.; An, H.L.; Luo, S.C.; Tang, T.K.; Su, W.F. Novel 3D Neuron Regeneration Scaffolds Based on Synthetic Polypeptide Containing Neuron Cue. Macromolecular bioscience, **2018,** *18(3),* 1700251. DOI: 10.1002/mabi.201700251.

(102) Genchi, G.G.; Ciofani, G.; Polini, A.; Liakos, I.; Iandolo, D.; Athanassiou, A.; Pisignano, D.; Mattoli, V.; Menciassi, A. PC12 neuron-like cell response to electrospun poly (3-hydroxybutyrate) substrates. *J. Tissue Eng. Regener. Med.* **2015,** *9(2),* 151-161. DOI: 10.1002/term.1623.

(103) Patel, N.; Poo, M.M. Orientation of neurite growth by extracellular electric fields. *J. Neurosci.* **1982,** *2(4),* 483-496. DOI: 10.1523/JNEUROSCI.02-04-00483.1982.

(104) Kotwal, A.; Schmidt, C.E. Electrical stimulation alters protein adsorption and nerve cell interactions with electrically conducting biomaterials. *Biomaterials,* **2001,** *22(10),* 1055-1064. DOI: 10.1016/S0142-9612(00)00344-6.

(105) Basser, P.J. Focal magnetic stimulation of an axon. *IEEE Trans. Biomed. Eng.* **1994,** *41(6),* 601-606. DOI: 10.1109/10.293248.

(106) Kimura, K.; Yanagida, Y.; Haruyama, T.; Kobatake, E.; Aizawa, M. Electrically induced neurite outgrowth of PC12 cells on the electrode surface. *Med. Biol. Eng. Comput.* **1998,** *36(4),* 493-498. DOI: 10.1007/BF02523221.

(107) Traynor, A.E.; Schubert, D. Phospholipases elevate cyclic AMP levels and promote neurite extension in a clonal nerve cell line. *Brain Res.* **1984,** *316(2),* 197-204.

(108) Kimura, K.; Yanagida, Y.; Haruyama, T.; Kobatake, E.; Aizawa, M. Gene expression in the electrically stimulated differentiation of PC12 cells. *J. Biotechnol.* **1998,** *63(1),* 55-65. DOI: 10.1016/S0168-1656(98)00075-3.

(109) Cavalie, A.; Berninger, B.; Haas, C.A.; Garcia, D.E.; Lindholm, D.; Lux, H.D. Constitutive upregulation of calcium channel currents in rat phaeochromocytoma cells: role of c-fos and c-jun. *J. Physiol.* **1994,** *479(1),* 11-27. DOI: 10.1113/jphysiol.1994.sp020274.

(110) Rosen, L.B.; Greenberg, M.E. Stimulation of growth factor receptor signal transduction by activation of voltage-sensitive calcium channels. *Proc. Natl. Acad. Sci.* **1996,** *93(3)*, 1113-1118.

Table of Contents Graphic and Synopsis

Electrically conductive, porous, mechanically strong and bioactive core-sheath electrospun MEH-PPV:PCL nanofibres were surface functionalized using APTES and 1,6-hexanediamine to incorporate amine functionality, which provides necessary bioactive sites for better 3T3 fibroblast adhesion, spreading and proliferation and moderate PC12 differentiation. Electrical stimulation along surface functionalization demonstrates enhanced neurite formation and neurite outgrowth on the surface functionalized meshes that is comparable to that on the collagen coated meshes under no electrical stimulation, while the best results are obtained on the collagen I coated nanofibres, indicating its potential in neural tissue engineering applications.